Cell Reports

Article

Auxin-dependent post-translational regulation of MONOPTEROS in the *Arabidopsis* root

Graphical abstract

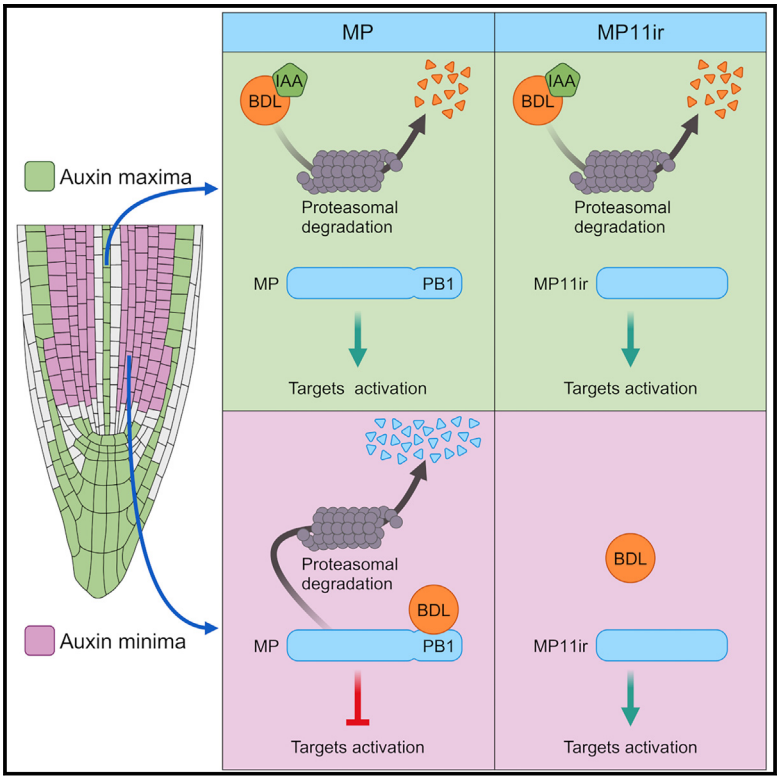

Highlights

- In roots, full-length MP and MP11ir isoform accumulation is post-translationally regulated
- Full-length MP protein is stable in tissues with high auxin
- At low auxin levels, full-length MP interactions with AUX/IAAs determine its degradation
- MP isoform regulation is required to control root development and sensitivity to auxin

Authors

Alex Cavalleri, Chiara Astori, Jekaterina Truskina, ..., Rahul Bhosale, Anthony Bishopp, Lucia Colombo

Correspondence

lucia.colombo@unimi.it

In brief

Cavalleri et al. show that in *Arabidopsis* roots, the accumulation of MP and MP11ir splicing isoform is post-translationally regulated. MP is stable in high-auxin tissues, whereas interaction with AUX/IAAs causes its degradation at low auxin levels. MP isoforms are required to ensure correct root development and sensitivity to auxin.

Cavalleri et al., 2024, Cell Reports *43*, 115083
December 24, 2024
https://doi.org/10.1016/j.celrep.2024.115083

CellPress

Cell Reports

CellPress
OPEN ACCESS

Article

Auxin-dependent post-translational regulation of MONOPTEROS in the *Arabidopsis* root

Alex Cavalleri,[1] Chiara Astori,[1] Jekaterina Truskina,[2] Mara Cucinotta,[1] Etienne Farcot,[3] Elina Chrysanthou,[4] Xiaocai Xu,[5] Jose M. Muino,[5] Kerstin Kaufmann,[5] Martin M. Kater,[1] Teva Vernoux,[2] Dolf Weijers,[6] Malcolm J. Bennett,[4] Rahul Bhosale,[4] Anthony Bishopp,[4] and Lucia Colombo[1,7,*]

[1]Department of BioScience, University of Milan, 20133 Milano, Italy
[2]Laboratoire Reproduction et Développement des Plantes, Université de Lyon, ENS de Lyon, CNRS, INRAE, 69342 Lyon, France
[3]School of Mathematical Sciences, University of Nottingham, NG7 2RD Nottingham, UK
[4]School of Biosciences, University of Nottingham, LE12 5RD Loughborough, UK
[5]Plant Cell and Molecular Biology, Institute of Biology, Humboldt-Universität zu Berlin, 10115 Berlin, Germany
[6]Laboratory of Biochemistry, Wageningen University, 6700 ET Wageningen, the Netherlands
[7]Lead contact
*Correspondence: lucia.colombo@unimi.it
https://doi.org/10.1016/j.celrep.2024.115083

SUMMARY

Auxin plays a pivotal role in plant development by activating AUXIN RESPONSE FACTORs (ARFs). Under low auxin levels, ARF activity is inhibited by interacting with Aux/IAAs. Aux/IAAs are degraded when the cellular auxin concentration increases, causing the release of ARF inhibition. Here, we show that levels of the ARF5/MONOPTEROS (MP) protein are regulated in a cell-type-specific and isoform-dependent manner. We find that the stability of MP isoforms is differentially controlled depending on the auxin level. The canonical MP isoform is degraded by the proteasome in root tissues with low auxin levels. While auxin sharpens the MP localization domain in roots, it does not do so in ovules or embryos. Our research highlights a mechanism for providing spatial control of auxin signaling capacity. Together with recent advances in understanding the tissue-specific expression and post-transcriptional modification of auxin signaling components, these results provide insights into understanding how auxin can elicit so many distinct responses.

INTRODUCTION

AUXIN RESPONSE FACTORs (ARFs) play a central role in the transcriptional response to auxin.[1] ARFs have partially overlapping expression patterns, providing them with the ability to cooperate for the regulation of different developmental processes.[2–4] Despite this, they also have specific and non-redundant activities, suggesting the existence of cell-type-specific auxin signaling circuits.[5] The five class A ARF proteins share a modular structure, with a B3-type DNA-binding domain (DBD) at the N terminus that mediates binding to AuxRE DNA motifs.[6,7] The central part (middle region [MR]) of the protein is an intrinsically disordered domain rich in glutamines and mediates transcriptional activation.[8,9] The C terminus harbors a type I/II PB1 domain responsible for ARF-ARF and ARF-Aux/IAA interactions.[10–12] In *Arabidopsis thaliana*, the Aux/IAA family comprises 29 proteins. These can interact with class A ARFs through their PB1 domain to repress their activity.[10,12–14] Indeed, due to the presence of an EAR motif, Aux/IAAs can recruit co-repressors, which in turn recruit chromatin modifiers to bring about repression.[15–17] The auxin signaling mechanism relies on the modulation of the interaction between ARFs and Aux/IAAs. Aux/IAAs show a meager ability to interact with class B and class C ARFs, making the current model of the auxin-mediated regulation of gene expression applicable only to class A ARFs.[18] Briefly, auxin promotes the interaction between Aux/IAAs and the intracellular auxin receptor TIR1, which is a member of the E3 ubiquitin ligase complex $SCF^{TIR/AFB}$.[19–22] In this context, Aux/IAAs are ubiquitinated and targeted for proteasomal degradation, allowing class A ARFs to promote the expression of target genes.

One of the best-characterized class A ARFs is ARF5/MONOPTEROS (ARF5/MP), which is a major effector of auxin signaling. MP plays a central role during embryogenesis and primary root formation,[23–26] post-embryonic root development,[27,28] vasculature tissue formation,[24,25,29] meristem maintenance, and flower[17,30–32] and ovule[33,34] formation. MP activity is regulated by interactions with Aux/IAA12/BODENLOS (BDL) in embryos,[26,35] and thus BDL confers auxin regulation to MP. Indeed, during embryo development, not only do MP and BDL directly interact through their PB1 domains, but BDL also works as a strong inhibitor of MP function at low auxin levels.[26]

Despite this evidence, the ability of MP to act in a vast range of developmental processes suggests that the mechanism through which it works could be highly dynamic and context dependent. In addition to BDL, MP interacts with all the other Aux/IAAs,[12] a fact that could, in part, explain this property. However, it was also shown that during ovule development, MP activates its targets in domains with low auxin levels. Particularly, it has been shown that MP function is regulated by alternative splicing (AS). This

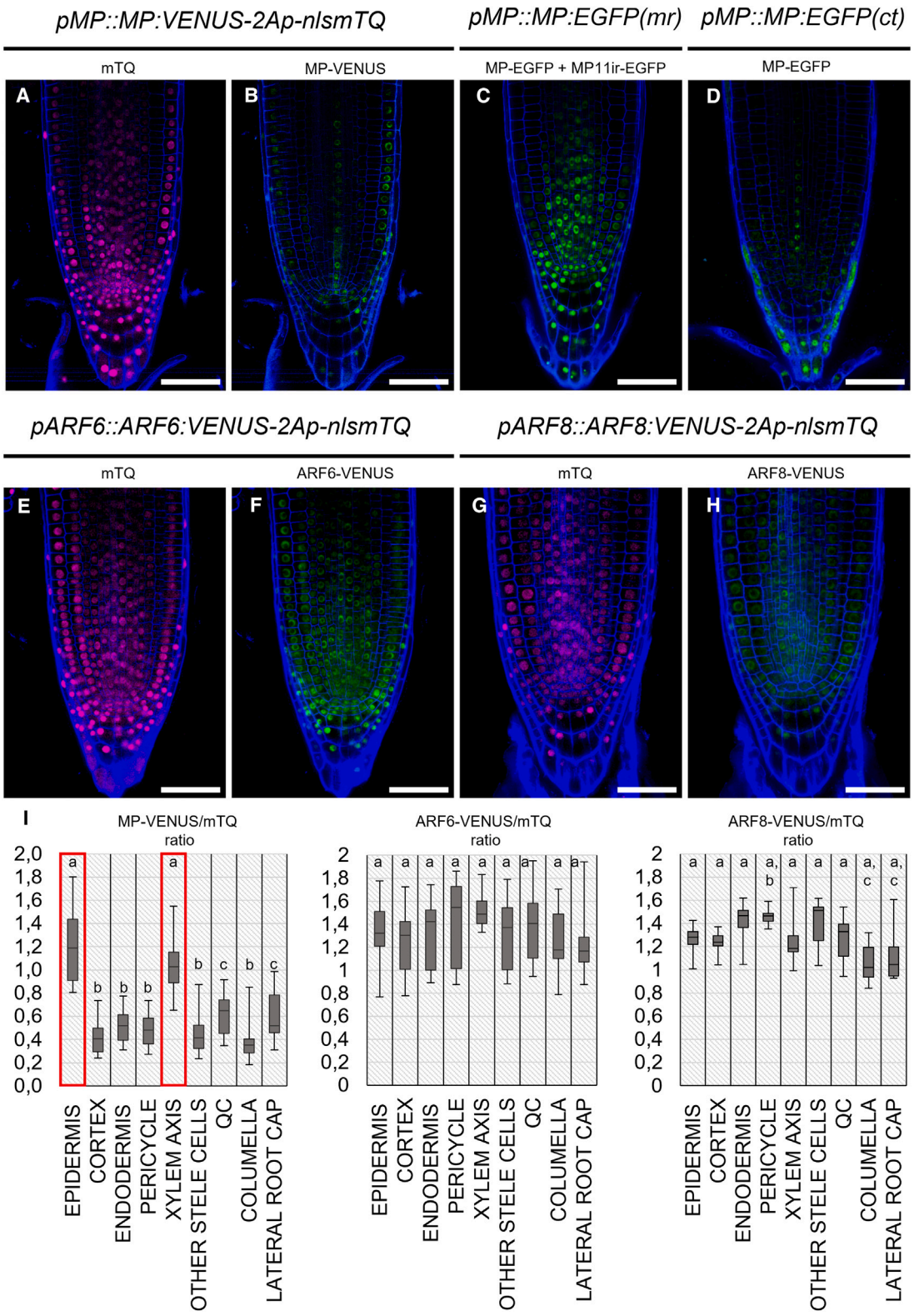

Figure 1. MP protein accumulation is post-translationally regulated

(A and B) *pMP::MP:VENUS-2Ap-mTQ* reporter line showing mTQ signal associating with *MP* transcription and translation (A) and the accumulation pattern of the MP-VENUS fusion protein (B).

(legend continued on next page)

process generates an alternative MP isoform named MP11ir that lacks the PB1 domain.[34] Interestingly, in this context, MP regulation mediated by Aux/IAAs seems not to be fundamental for its function.

Considering the ability of MP to coordinate various developmental processes, together with the emerging relevance of ARF post-transcriptional regulation, we decided to further investigate *MP* regulatory mechanisms. Studying the *MP* function in roots allowed us to demonstrate that its post-transcriptional regulation is further integrated with a post-translational modulation of its isoforms. We show that the two MP isoforms have different accumulation patterns. The canonical MP is stabilized in tissues with a high auxin content. By contrast, in tissues with low auxin, the accumulation of canonical MP is prevented by the interaction with BDL, which leads to MP proteasomal degradation. We provide evidence that supports a tissue- and organ-specific mechanism for the MP-BDL module.

RESULTS

Post-translational regulation modulates the levels of MP in roots

AS generates two distinct *MP mRNA* variants: canonical *MP* and an alternative transcript retaining the eleventh intron.[34] The translation of these *mRNA*s leads to the production of two functional MP protein isoforms, the full-length MP and the alternative MP11ir variant, lacking the PB1 domain.[34] We investigated the spatial differences in transcription, translation, and protein accumulation of the two *MP* isoforms in roots. We first verified that both isoforms were translated during seedling development by performing polysome profiling. In a similar manner to previous work in the inflorescence,[34] both *MP* and *MP11ir* were associated with light and heavy polysomes, indicating their translation (Figures S1A and S1B).

To study the spatial distribution of MP isoform accumulation, we analyzed two marker lines: *pMP::MP:VENUS-2Ap-mTURQUOISE* and *pMP::MP:EGFP(mr)*.[24] In the *pMP::MP:VENUS-2Ap-mTQ* line, the viral 2A peptide (2Ap) works as a self-cleaving peptide by inducing ribosomal skipping during translation, leading to the production of two independent proteins from the same transcript.[36,37] The presence of the 2Ap allows us to simultaneously visualize *MP* transcription/translation domain (mTQ signal) and canonical MP protein accumulation (MP-VENUS signal) (Figure S1C). The second reporter line used, *pMP::MP:EGFP(mr)*, contains the *EGFP* sequence in the MR domain of *MP*, upstream of the differentially spliced *MP* eleventh intron. This leads to the translation of two distinct fusion proteins: the canonical MP-EGFP and the alternative MP11ir-EGFP. Therefore, the EGFP pattern is the result of a combination of both MP isoforms (Figures S1C and S1D).

By analyzing the mTQ signal in roots of *pMP::MP:VENUS-2Ap-mTQ* seedlings, we detected *MP* transcription and translation in most cells of the root apical meristem (RAM), similar to what has been previously described (Figure 1A).[3,38,39] Similarly, the signal arising for the combination of MP-EGFP and MP11ir-EGFP fusion proteins from *pMP::MP:EGFP(mr)* showed an analogous expression profile (Figure 1C). By contrast, in the *pMP::MP:VENUS-2Ap-mTQ* line, we observed that MP-VENUS accumulated in a narrower domain, which comprises the xylem axis, the quiescent center (QC), and the epidermis (Figures 1B, S2A, and S2B). We confirmed this observation by analyzing an additional MP protein reporter line, *pMP::MP:EGFP(ct)*, which carries the *EGFP* at the *MP* 3′ end as for *MP:VENUS* in the *pMP::MP:VENUS-2Ap-mTQ* line. Consistently, MP-EGFP and MP-VENUS proteins accumulated similarly in the RAM (Figures 1B and 1D). This discrepancy between patterns of translation and protein accumulation suggests the post-translational modification of the canonical MP isoform in this tissue.

To evaluate whether this post-translational regulation was specific to MP or shared with other class A ARFs, we generated similar reporter lines for *ARF6* and *ARF8.* In both cases, we observed identical translational domains and protein accumulation patterns (Figures 1E–1H).

We analyzed the tissue specificity of MP, ARF6, and ARF8 by quantifying the VENUS/mTQ signal ratio among the different cell types within the RAM. We observed higher levels of MP protein (higher VENUS/mTQ ratio) occurring in the epidermis and xylem, while all other measured tissues showed a lower ratio (Figure 1I). To exclude that the observed reduction in MP-VENUS accumulation was due to a possible tissue-specific regulation of *MP* transcription, we also evaluated solely the mTQ signal in the same tissues. In the *pMP::MP:VENUS-2Ap-mTQ* reporter system, the mTQ is translated after the MP protein is produced.[40] Therefore, the mTQ pattern depicts the domain of canonical *MP* translation. No differences in mTQ signal were found among the epidermis, cortex, endodermis, pericycle, xylem axis, and stele cells (Figure S2C). A higher mTQ signal was observed in the columella, lateral root (LR) cap, and QC (Figure S2C). This expression pattern is comparable with the *MP* expression profile

(C) *pMP::MP:EGFP(mr)* reporter line pattern displays the combined output of both MP-EGFP and MP11ir-EGFP fusion proteins.
(D) Accumulation pattern of the MP-EGFP fusion protein (D), from the *pMP::MP:EGFP(ct)* line, is similar to that of MP-VENUS (B).
(E–H) *pARF6::ARF6:VENUS-2Ap-mTQ* reporter line (E and F). *pARF8::ARF8:VENUS-2Ap-mTQ* reporter line (G and H). In both cases, no differences in the domains of transcription and translation (E and G) or protein accumulation (F and H) have been observed.
(I) MP, ARF6, and ARF8 protein accumulation in the different root tissue calculated as a VENUS/mTQ signal intensity ratio in individual nuclei. For the *pMP::MP:VENUS-2Ap-mTQ* reporter line, the measurements were performed on 27, 31, 31, 28, 37, 53, 11, 23, and 32 nuclei from the epidermis, cortex, endodermis, pericycle, xylem axis, other stele cells, QC, columella, and lateral root cap, respectively, belonging to five different root meristems. For the *pARF6::ARF6:VENUS-2Ap-mTQ* reporter line, the measurements were performed on 38, 27, 20, 15, 27, 22, 9, 16, and 21 nuclei from the epidermis, cortex, endodermis, pericycle, xylem axis, other stele cells, QC, columella, and lateral root cap, respectively, belonging to five different root meristems. For the *pARF8::ARF8:VENUS-2Ap-mTQ* reporter line, the measurements were performed on 21, 17, 16, 10, 10, 17, 5, 6, and 18 nuclei from the epidermis, cortex, endodermis, pericycle, xylem axis, other stele cells, QC, columella, and lateral root cap respectively, belonging to four different root meristems. Boxplot elements correspond to the following: center line = median; box limits = interquartile range; whiskers = lowest and highest values in the 1.5 interquartile range. Letters over boxplots indicate the statistical difference as determined by a one-way ANOVA with the post hoc Tukey honestly significant difference (HSD) test with $p < 0.05$.
Scale bars: 50 μm.

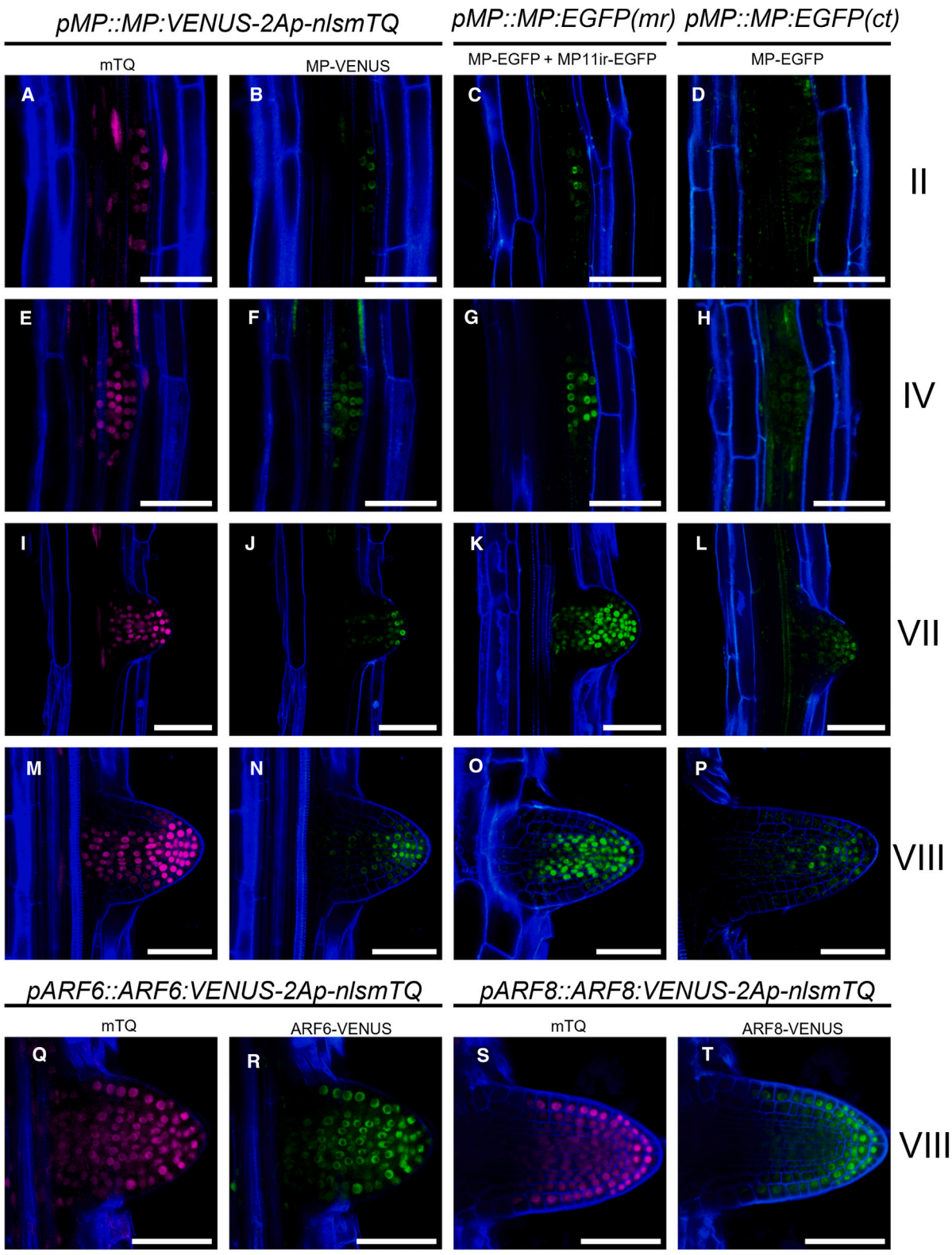

Figure 2. MP pattern during lateral root organogenesis

(A–P) Lateral root primordia at stages II (A–D), IV (E–H), VII (I–L), and VIII (M–P) from *pMP::MP:VENUS-2Ap-mTQ* reporter line (A, B, E, F, I, J, M, and N), *pMP::MP:EGFP(mr)* reporter line (C, G, K, and O), and *pMP::MP:EGFP(*ct*)* reporter line (D, H, L, and P). At stages II and IV, *MP* is transcribed and translated in the

(legend continued on next page)

in a root single-cell RNA sequencing (RNA-seq) dataset,[41] confirming that the mTQ signal correctly reflects the *MP* transcriptional profile.

Concerning ARF6 and ARF8, in both cases we measured a similar VENUS/mTQ ratio in all RAM tissues (Figure 1I).

To verify whether the discrepancy observed between MP translation and protein accumulation was specific to the RAM or if it was reflecting a more general principle, we analyzed MP reporter lines during LR organogenesis. At stages II and IV, *MP* was transcribed and translated in all cells of LR primordia (Figures 2A and 2E), and no differences were observed between the accumulation patterns of the different MP isoforms (Figures 2B–2D and 2F–2H). At stages VII–VIII, while the mTQ and the *pMP::MP:EGFP(mr)* reporter remained detectable in the whole primordium (Figures 2I, 2K, 2M, and 2O), the canonical MP protein accumulated specifically at its apex (Figures 2J, 2L, 2N, and 2P).

This behavior was specific for MP, as no differences were observed between translation and protein accumulation patterns of ARF6 and ARF8 during any stage of LR primordia development (Figures 2Q–2T).

As we had observed that this divergence between the domain in which MP is translated and protein accumulates in roots, we speculated that it may also occur in other developmental contexts, such as ovule and embryo development. In contrast to our observations in roots, *pMP::MP:VENUS-2Ap-mTQ* analysis in ovules showed that MP-VENUS accumulation was similar to the *pMP::MP:EGFP(mr)* pattern. Here, both reporter lines accumulate in the chalazal region of the ovule (Figures S2D–S2F). We next examined early stages of embryo development and observed that, even in this case, MP reporters overlap (Figures S2G–S2L), suggesting that this mechanism of MP post-translational regulation may be specific to roots.

MP is stable in tissues with high auxin levels

Our analysis revealed that canonical MP protein is stable only in a subset of root cells (Figures 1 and 2). The domains associated with MP protein stability in the RAM are regions that have been previously described as areas of high auxin signaling output.[42–45] Consistently, in LR primordia, MP accumulates in cells with high auxin. From stage I to IV, LR primordia are characterized by high auxin levels throughout the primordia, whereas auxin is concentrated only in a few cells in the primordium apex from stage V to VIII,[46,47] following a pattern similar to the one observed for canonical MP. To determine if the tissue specificity of MP accumulation in the RAM was associated with high auxin content, we evaluated auxin levels in the root tip by analyzing the R2D2 reporter line.[42] We measured the mDII-tdTOMATO/DII-VENUS ratio in the different cell types of the RAM. Our analysis confirmed that the tissues showing MP accumulation (epidermis and xylem axis) (Figure 1I) presented the highest mDII-tdTOMATO/DII-VENUS ratio as a result of the enhanced DII-VENUS degradation occurring in such tissues (Figures 3A and 3B).

To explore whether high auxin levels were controlling MP accumulation, we treated *pMP::MP:VENUS-2Ap-mTQ* seedlings with indole-3-acetic acid (IAA) and compared mTQ and MP-VENUS patterns between mock- and IAA-treated samples. While auxin treatment did not alter the pattern of *MP* transcription and translation (Figures 3C and 3E), it caused an expansion of the MP-VENUS domain (Figures 3D, 3F, and 3G), highlighting the ability of cells with higher auxin levels to exhibit stable accumulation of MP. Even though MP resulted in the only observed ARF showing a discrepancy between the domains of expression and protein accumulation, we also tested whether ARF6 and ARF8 protein stability could be controlled by auxin levels. We found no statistically significant differences in ARF6 and ARF8 accumulation patterns after IAA treatment (Figures S3A–S3H, S3M, and S3N).

MP is degraded by the proteasome through ubiquitin-dependent proteolysis

The observation that MP accumulated only in domains of high auxin concentration led us to investigate the possible mechanism underlying the absence of MP in tissues with low auxin. The mTQ signal from the *pMP::MP:VENUS-2Ap-mTQ* line (Figure 1A) showed that MP is translated in cells with both low and high auxin concentrations, implying that the absence of MP in cells with low auxin could be associated with a post-translational regulation affecting MP stability. We hypothesized that the canonical MP protein could be actively degraded by the proteasome in domains of low auxin in the RAM. To test whether the MP pattern was controlled by proteasomal degradation, *pMP::MP:VENUS-2Ap-mTQ* seedlings were treated with bortezomib (BTZ), an inhibitor of proteasome activity.[48–50] Proteasome inhibition promoted MP-VENUS accumulation; MP protein was visible throughout the entire domain in which it was translated (Figures 4A–4D and 4K). To characterize whether the degradation of the canonical MP protein in low auxin conditions was associated with ubiquitin-dependent or -independent proteolysis, we treated *pMP::MP:VENUS-2Ap-mTQ* seedlings with MG132 or PYR41. MG132 is able to block both ubiquitin-dependent and -independent proteolysis similarly to BTZ.[50] Instead, PYR41 acts as an inhibitor of the ubiquitin-activating enzyme E1, thus allowing selective blocking of ubiquitin-dependent degradation.[51,52] MG132 treatment significantly increased MP-VENUS accumulation (Figures 4E–4H and 4L). Interestingly, MP-VENUS stability also increased after treatment with PYR41 (Figures 4E, 4F, 4I, 4J, and 4L). These results not only support the role of protein degradation in the regulation of the MP pattern but also indicate that MP might be a direct or indirect target of a ubiquitin ligase. By analyzing the MP protein sequence using the ubiquitin-site predictor "BDM-PUB,"[53] we identified several putative sites for ubiquitin conjugation, suggesting MP's potential ability to be directly ubiquitinated (Table S1).

whole primordium (A and E), and no differences were observed between MP isoform patterns (B–D and F–H). At stages VII and VIII, while the mTQ signal is still visible in the whole primordium (I and M), similarly to the *pMP::MP:EGFP(mr)* line (K and O), the canonical MP fusion proteins accumulate preferentially at the primordium apex (J, N, L, and P).

(Q–T) *pARF6::ARF6:VENUS-2Ap-mTQ* (Q and R) and *pARF8::ARF8:VENUS-2Ap-mTQ* (S and T) reporter lines in lateral root primordia at stage VIII. No differences among the domains of transcription and translation and fusion protein accumulation have been observed for either ARF6 (Q and R) or ARF8 (S and T). Scale bars: 50 μm.

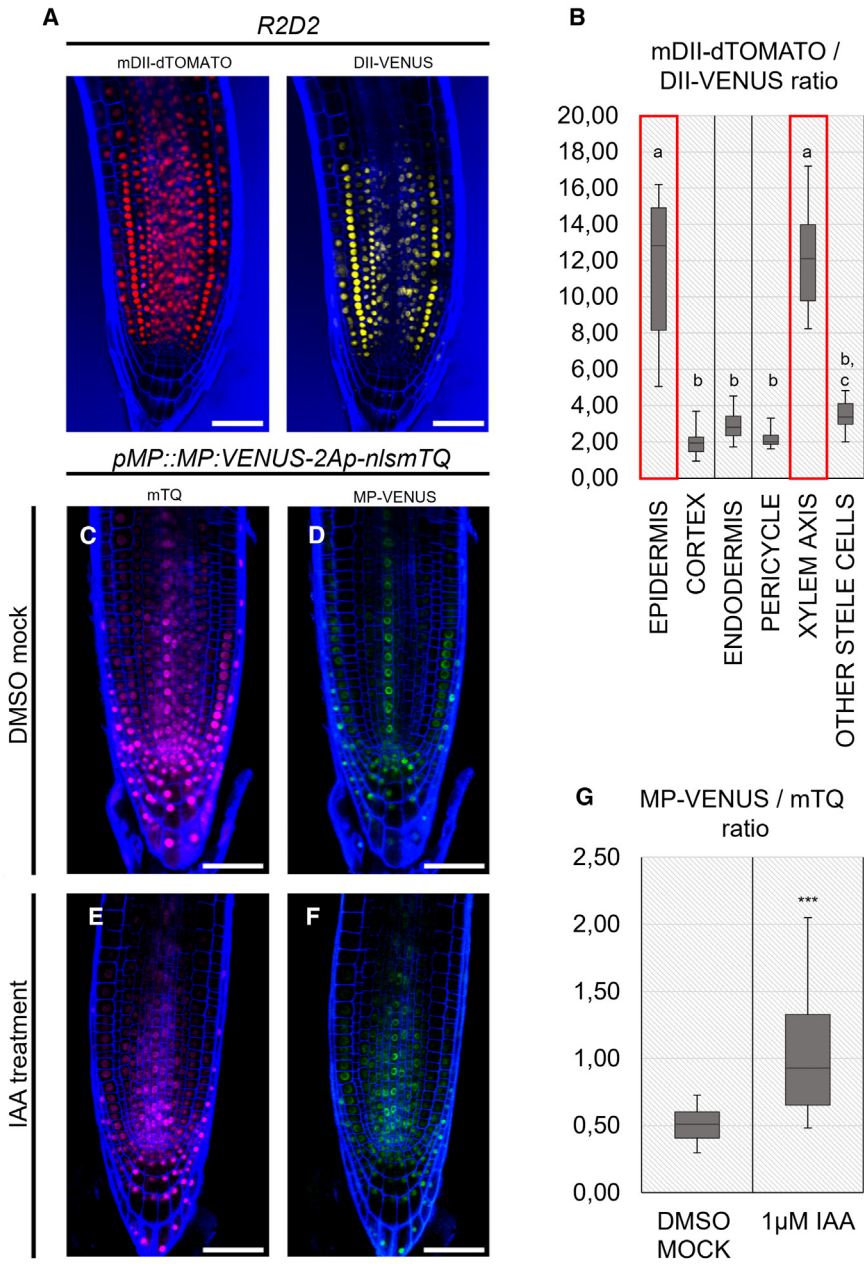

Figure 3. MP accumulation is enhanced by high auxin levels

(A and B) Auxin levels in the RAM were visualized using the R2D2 reporter (A) and by calculating the mDII-dTOMATO/DII-VENUS ratio in single nuclei of the different tissues showing R2D2 expression (B). The measurements were performed on 19, 66, 25, 31, 21, and 27 nuclei from the epidermis, cortex, endodermis, pericycle, xylem axis, and other stele cells, respectively, belonging to five different root meristems. Boxplot elements correspond to the following: center line = median; box limits = interquartile range; whiskers = lowest and highest values in the 1.5 interquartile range. Letters over boxplots indicate the statistical difference as determined by a one-way ANOVA with the post hoc Tukey HSD test with $p < 0.05$.

(C–G) 4 hour 1 μM IAA treatment on *pMP::MP:VENUS-2Ap-mTQ* reporter line 5-day-old seedlings. mTQ signal (*MP* transcriptional and translation) and MP-VENUS fusion protein in mock condition (C and D) and IAA treatment (E and F) are compared.

(G) Signal intensity measurements between mock and IAA treatment calculated as VENUS/mTQ ratio in RAM vascular cylinder. Measurements were performed on 15 different plants for each treatment condition. Boxplot elements correspond to the following: center line = median; box limits = interquartile range; whiskers = lowest and highest values in the 1.5 interquartile range. The asterisks over the boxplots indicate the statistical difference as determined by a Student's t test (two-tailed distribution, homoscedastic) confronting the mock with the treatment condition. ***$p < 0.001$. Experiment was performed twice with similar results. Scale bars: 50 μm.

Finally, we evaluated whether ARF6 and ARF8 could also be regulated by proteasomal degradation in the root apex. No statistically significant differences in ARF6 and ARF8 levels were detected between mock- and BTZ-treated roots (Figures S3A–S3D and S3I–S3N), suggesting that the auxin-dependent post-translational regulation is specific for MP.

The interaction between MP and BDL promotes MP degradation in cells with low auxin

Despite proteasomal degradation in low-auxin areas of the reporter for canonical MP, the pattern of the *pMP::MP:eGFP(mr)* reporter line (Figure 1C) is present throughout the root tip. This suggests that the MP11ir isoform is uncoupled from proteasomal regulation and that its stability must therefore be independent of auxin concentration. MP and MP11ir differ in the presence of the PB1 domain, which mediates the interaction with Aux/IAAs.[34,54] We therefore speculated that the presence of the PB1 domain and its ability to bind Aux/IAAs could be important for regulating MP degradation. To test the hypothesis that Aux/IAA levels determine MP degradation, we analyzed MP accumulation in the presence of the auxin-insensitive bodenlos (bdl) mutant protein. The bdl mutant protein remains bound to MP through its PB1 domain even in cells with high auxin concentrations due to its enhanced stability.[55] We crossed a *GR:bdl*-inducible line[26] with *pMP::MP:VENUS-2Ap-mTQ* and compared the *MP* transcriptional and translational domains with MP-VENUS accumulation upon dexamethasone (DEX) induction. No differences were detected in the domain of *MP* transcription and translation in association with GR-bdl induction (Figures 5A and 5C). However, we observed that MP-VENUS accumulation was reduced upon DEX treatment (Figures 5B, 5D, and 5G). An MP-VENUS signal was detected in only a few cells, including those in the QC and part of the columella (Figure 5D).

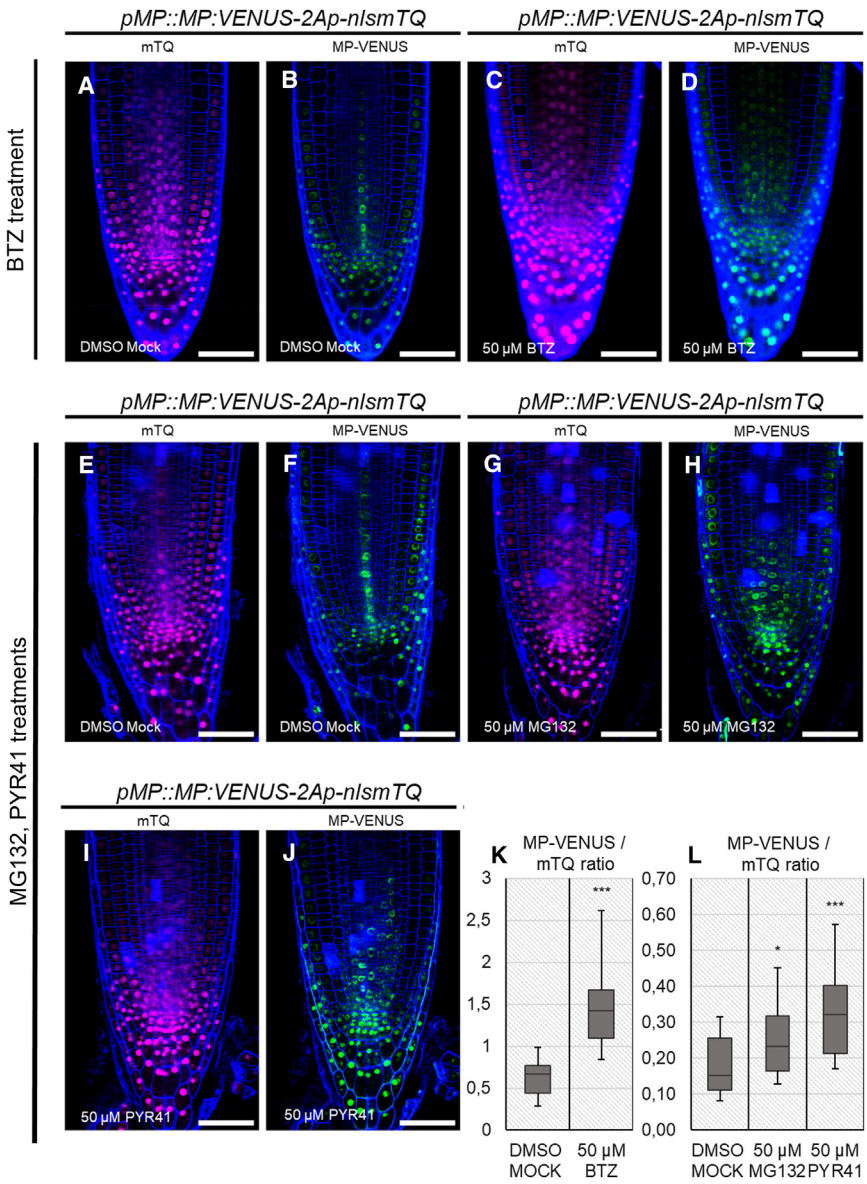

Figure 4. Proteasome inhibition restores MP pattern

(A–D) *pMP::MP:VENUS-2Ap-mTQ* 5-day-old seedlings treated for 4 h with mock solution (A and B) or 50 μM bortezomib (BTZ) (C and D), showing the mTQ pattern (A and C) and MP-VENUS domain (B, D).

(E–J) Mock (E and F), MG132 (G and H), and PYR41 (I and J) 4 h treatments on 5-day-old *pMP::MP:VENUS-2Ap-mTQ* seedlings. mTQ signal in mock (E), MG132 (G), and PYR41 (I) and MP-VENUS pattern in mock (F), MG132 (H), and PYR41 (J). Proteasome or ubiquitin conjugation inhibition allows MP-VENUS fusion protein accumulation (D, H, and J) with respect to the mock control (B and F). By contrast, the MP transcriptional and translational domain (mTQ signal) is not altered between mock (A and E) and treatment conditions (C, G, and I).

(K and L) Signal intensity measurements (VENUS/mTQ ratio) in RAM vascular cylinder between mock and BTZ treatment. Measurements were performed on 9 and 11 different roots for mock and BTZ conditions, respectively (K). The experiment was performed twice, with similar results. VENUS/mTQ signal ratio measurements in RAM vascular cylinder between mock, MG132, and PYR41 treatments. Measurements have been performed on 17, 23, and 16 different plants for mock, MG132, and PYR41 treatments, respectively, in two biological replicates (L). Boxplot elements correspond to the following: center line = median; box limits = interquartile range; whiskers = lowest and highest values in the 1.5 interquartile range. The asterisks over the boxplots indicate the statistical difference as determined by a Student's t test (two-tailed distribution, homoscedastic) confronting the mock with each treatment condition. *$p < 0.05$ and ***$p < 0.001$. Scale bars: 50 μm.

To verify if the decrease in MP-VENUS upon GR-bdl induction was directly related to the ubiquitination process, we performed a combined treatment with both DEX and PYR41. We observed that impairing ubiquitin conjugation prevented the reduction of MP-VENUS associated with GR-bdl induction (Figures 5C–5G). Finally, to exclude that the observed changes in MP-VENUS accumulation were due to changes in the auxin pattern caused by GR-bdl induction, we crossed the *GR:bdl* line with the *R2D2* reporter. After DEX treatment, the auxin accumulation pattern remained equal to the one observed in the mock control (Figures S4A–S4D). Auxin accumulated in the epidermis and the xylem axis in both mock- and DEX-treated roots (Figures S4B, S4D, and S4E). These results suggest that the constitutive binding of BDL to the canonical MP isoform leads to its degradation via ubiquitin-dependent proteolysis.

Auxin responsiveness differs between MP isoforms

After observing that the stability of MP in roots is dependent on the concentration of IAA within a cell (Figures 1 and 3), we focused our attention on the effect that MP isoforms could have on root growth and development. Since the DBD is identical in both isoforms, they will likely target the same downstream response genes. However, MP11ir lacks the PB1 domain and is unable to interact with Aux/IAAs; therefore, it is unlikely to be regulated by auxin.

To further investigate MP isoform functionality, we took advantage of lines in which either the MP or the MP11ir variants were used to complement the weak *mpS319* mutant (referred to as *pMP::MP* and *pMP::MP11ir*, respectively).[34] Even though *pMP::MP11ir* lines have a lower expression level of *MP* mRNA in roots when compared with *pMP::MP* (Figure S5A), both lines partially rescued the rootless phenotype associated with the *mpS319* mutation (Figure S5B). In both cases, the root development process occurred similarly, confirming that both isoforms

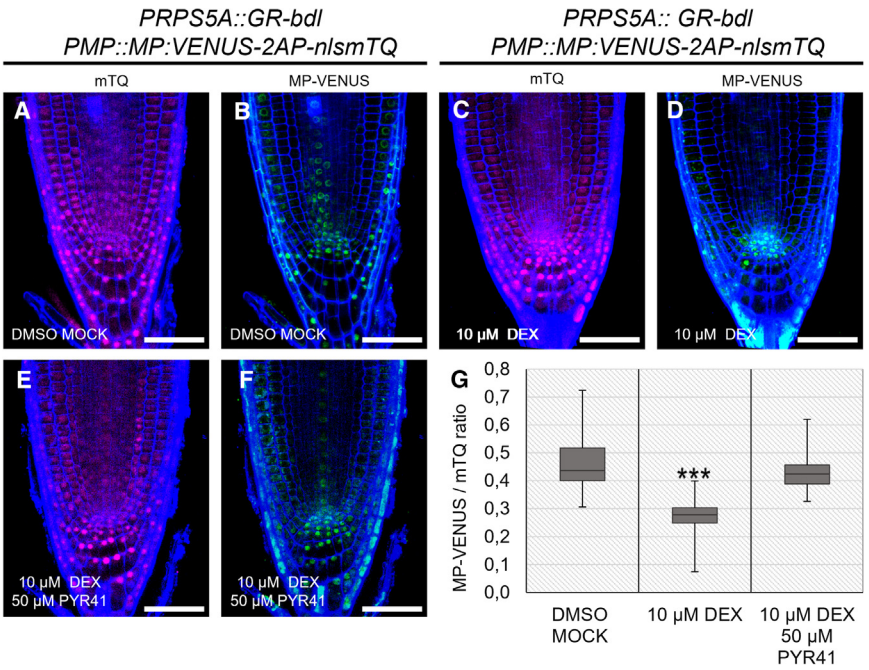

Figure 5. Induction of bdl enhances ubiquitin-dependent MP proteolysis

(A–D) 4 hour 10 µM DEX induction on *pRPS5A::GR-bdl/pMP::MP:VENUS-2Ap-mTQ* 5-day-old seedlings, showing mTQ and MP-VENUS patterns in mock treatment (A and B) or DEX treatment (C and D). DEX allows bdl translocation to the nucleus.

(E and F) 4 h combined induction of bdl by DEX treatment and inhibition of ubiquitin-dependent proteolysis (PYR41 treatment) on *pRPS5A::GR-bdl/pMP::MP:VENUS-2Ap-mTQ* 5-day-old seedlings.

(E and F) Signals in DEX/PYR41 treatment (E and F) are confronted with the ones in mock (A and B) and DEX (C and D) conditions.

(G) VENUS/mTQ signal ratio measurements in the RAM between mock, DEX, and DEX/PYR41 treatments. Induction of bdl statistically decreased MP protein accumulation, while no statistically significant differences were observed when bdl induction was performed in association with PYR41 treatment. Measurements have been performed on 35, 37, and 25 different plants among three biological replicates for mock, DEX, and DEX/PYR41 treatments, respectively. Boxplot elements correspond to the following: center line = median; box limits = interquartile range; whiskers = lowest and highest values in the 1.5 interquartile range. The asterisks over the boxplots indicate the statistical difference as determined by a Student's t test (two-tailed distribution, homoscedastic) confronting the mock with each treatment condition. ***$p < 0.001$. Scale bars: 50 µm.

could provide an MP function and activate downstream targets. Interestingly, we measured a statistically significant increase in root length in *pMP::MP11ir* with respect to the wild type and *pMP::MP* lines (Figures S5C–S5F).

Since MP was previously described to be involved in vasculature development (as reviewed in Yang and Wang[56]), we evaluated the accuracy of the vasculature pattern of these plants. We observed minor defects in both complementation lines; however, these alterations were more prevalent in *MP11ir* (Figure S5G). As we observed these fine differences in root development between the lines, we also enquired about the impact that the presence of only one isoform or the other could have on the root meristem organization and maintenance. While many root tips appeared similar to the wild type, with slight defects in both complementation lines, we observed a relevant percentage of highly disorganized root tips in *pMP::MP11ir* (16/68 in the *pMP::MP11ir* line compared with 3/57 in the *pMP::MP* line) (Figures 6A–6D). These defects were predominantly related to the columella, and to obtain a more accurate description of this phenotype, we evaluated the morphology of these cells. In both wild type and *pMP::MP*, we could measure a clear difference in cell elongation between the first layers of the columella (predominantly between c1-c2 and c2-c3 layers) as a consequence of cellular differentiation (Figure 6E). Even though this trend was maintained in all the genotypes, in *pMP::MP11ir*, cell elongation between the first columella layers was altered (Figure 6E), suggesting an impairment in the cellular differentiation or organization.

These results indicate that downstream responses of MP might not be correctly modulated when part of the MP activity is not regulated by auxin. To corroborate this observation, we performed RNA-seq analysis on *pMP::MP* and *pMP::MP11ir* roots. Similar numbers of genes were differentially expressed ($-0.6 \leq$ log2 fold change [log2FC] ≥ 0.6, false discovery rate [FDR] ≤ 0.05) in *pMP::MP* and *pMP::MP11ir* lines when compared to the wild type (Figure S6A; Table S2). However, differentially expressed gene (DEG) Plant Ontology enrichment analysis revealed that only a very small number of root-specific categories were impaired in *pMP::MP* (Figures 6F; Table S3). By contrast, *pMP::MP11ir* DEGs were statistically enriched in categories associated with xylem, vasculature, meristem, and stele development, a result in line with the phenotypical differences observed between the two lines (Figures 6G; Table S4). Previously, a list of 106 rapidly induced MP target genes was reported,[24] and we decided to verify the expression of these genes in our datasets. In both *pMP::MP* and *pMP::MP11ir*, 25 of these genes were found to be differentially expressed ($0 <$ log2FC > 0, FDR ≤ 0.05) (Figure S6B; Table S5). Interestingly, while only 11 genes were upregulated in *pMP::MP*, 17 genes showed an increase in expression in *pMP::MP11ir* with respect to the wild type (Figure S6B; Table S5). In particular, 9 genes were only differentially expressed in one of the two complementation lines (Figure S6C; Table S5). This suggests that MP and MP11ir have specific and non-redundant functions for the activation of downstream targets.

Finally, in light of the different impacts that auxin levels have on MP isoform accumulation, we also hypothesized that the presence of only one isoform or the other could be transduced in a different plant responsiveness to auxin. We grew our lines on media supplemented with different IAA concentrations (10, 100, 300, and 1,000 nM) and followed root growth from 2 to 5 days after germination. Wild-type and *pMP::MP* plants were

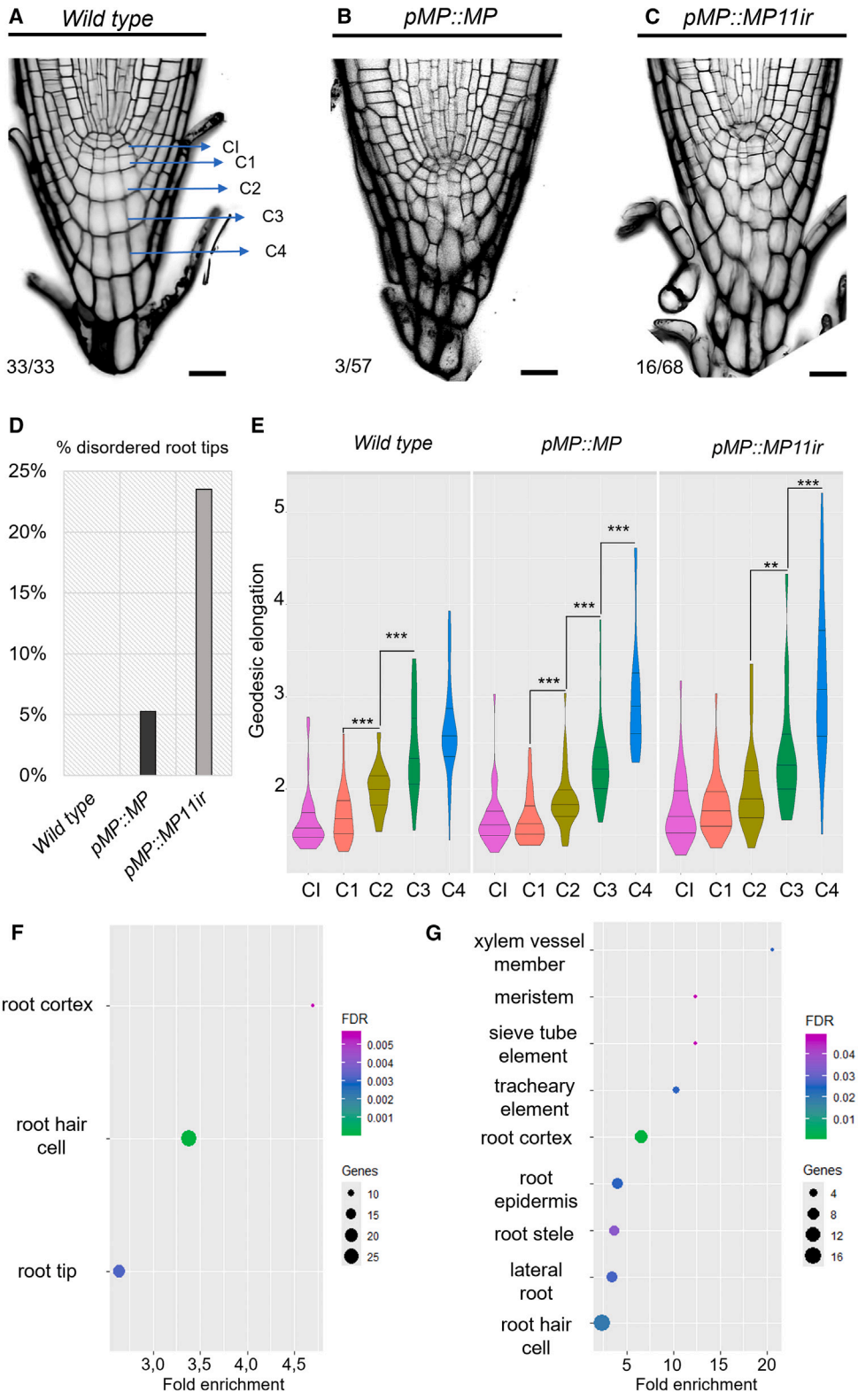

(legend on next page)

both responsive to exogenous IAA even at the lowest concentration (10 nM), as we measured a significant decrease in primary root length (Figure S7A). By contrast, in *pMP::MP11ir* plants, no significant differences were observed in primary root length at 10 and 100 nM IAA concentrations (Figures S7A and S7B). At the highest IAA concentrations (300 and 1,000 nM), all the genotypes showed a reduction in primary root length, albeit with milder effects in *pMP::MP11ir* plants (Figures S7C and S7D). Together, these observations suggest that the post-transcriptional regulation of MP could modulate the root development and responsiveness to auxin.

Conceptual investigation of the impact that auxin-dependent MP degradation has on auxin output

Collectively, these data show that the MP11ir isoform is insensitive to auxin and mediates an auxin-independent MP output. The effect that degradation of the canonical isoform of MP has on signaling output is less clear. The current interpretation of the auxin signaling pathway relies on the assumption that the ability of ARFs to activate/repress target genes depends on their interaction with Aux/IAA proteins. Moreover, the degradation rates of the components of the auxin signaling machinery are usually considered linear.[58] By contrast, the outcome associated with a *scenario* in which ARF stability is dependent on the concentration of Aux/IAAs is not obvious and may require additional actors. To explore this experimentally would require further screening or the analysis of a range of MP isoforms with varying degrees of auxin-dependent degradation, and no such material exists. To explore the effect that the auxin-dependent MP degradation might have on the activation of target gene expression, a mathematical model was developed. This model simulates the response of a hypothetical mRNA target to auxin. It relies on a minimal set of assumptions (Methods S1) and includes MP degradation occurring via binding to Aux/IAAs, which are then targeted for degradation in an auxin-dependent manner. We simulated the output in response to a pulse of auxin and then explored the consequence of varying the degradation rate of ARF by binding to Aux/IAA, defined by the parameter VARF. Higher values of VARF correspond to the highest rates of MP degradation. Our simulations revealed that increasing VARF led to a lower level of ARF under low auxin, with only modest changes in ARF levels under high auxin, which is similar to what was observed experimentally for the canonical MP isoform. More interestingly, the model showed that ARF degradation regulated by auxin levels can indeed modulate the expression of target genes. Simulations for output revealed a sharper response to auxin with increasing VARF, with cells only responding to higher concentrations of auxin, and the auxin response switching off more rapidly with decreasing concentrations of auxin (Figure 7A). These simulations present a conceptual framework whereby altering the degradation of an individual ARF, auxin can attenuate its responsiveness to convert a broad peak of auxin into a sharper output. In our experimentation, we only observed this degradation in MP, but it could hypothetically occur in any class A ARF.

DISCUSSION

We show that in roots, there are two MP isoforms, and these have differential stability depending on the auxin concentration. The PB1 domain is present in canonical MP but lacking in MP11ir. This domain determines the protein stability of the canonical isoform in an auxin-dependent manner. We propose that through binding to the PB1 domain, BDL, or potentially other Aux/IAAs, causes MP degradation by the 26S proteasome in regions of low auxin. In this scenario, the binding of Aux/IAAs to MP can modulate its protein stability, essentially restricting the canonical MP isoform to cells with high auxin. Firstly, we observed that increasing the IAA levels enhanced MP accumulation. Then, we tested the effect that inhibition of protein degradation has on MP patterns, observing an expansion of its accumulation domain. Finally, we note that MP degradation can be enhanced by the induction of the bdl mutant protein, which cannot directly interact with the $SCR^{TIR1/AFB}$ E3 complex.[35,59] From all these observations, we hypothesize that Aux/IAAs, once bound to the MP PB1 domain, could be involved in the recruitment of additional and yet-unknown factors that commit MP to the degradation pathway (Figure 7B). Although our observations provide deeper insights, the mechanism of MP degradation needs further investigation. We hypothesize that Aux/IAAs could recruit to MP components of the ubiquitination machinery, such as F box proteins. This hypothesis is based on the observed effect that the inhibition of ubiquitin conjugation has on MP accumulation. Likewise, MP contains predicted ubiquitination sites.[60] Nevertheless, we believe that such factors should be different from the ones that make part of the classical auxin perception machinery. Indeed, the ability of the *bdl* mutant protein to trigger MP degradation suggests that such activity could not be performed by components such as TIR1. Recently, it was shown that different F box proteins can regulate ARF degradation. For instance, the F box

Figure 6. Root tip morphology in MP- and MP11ir-expressing lines

(A–D) Root tip cellular organization in wild-type, *pMP::MP*, and *pMP::MP11ir* lines (A–C) and percentage of roots with highly disorganized meristems in the same lines (D). The percentage of highly disorganized roots increases sensibly in *pMP::MP11ir.* Data are presented as percentage over the total number of observations.

(E) Morphology of different cell types within the columella of wild type, *pMP::MP*, and *pMP::MP11ir* presented as geodesic elongation. The cell types considered are the following: columella initials (CI) and the first (C1), second (C2), third (C3), and fourth (C4) layers of columella cells (A and E). Geodesic elongation increases among the different cell layers, moving from the CI toward the C4, in association with the cells becoming longer and narrower. *pMP::MP11ir* roots display a lower difference in cellular elongation between C1-C2 and C2-C3 layers with respect to that observed in wild type and *pMP::MP* (E). Measurements have been performed on 12, 15, and 14 different roots for wild type, *pMP::MP*, and *pMP::MP11ir*, respectively. Violin plot elements correspond to the following: center line = median, lower and higher lines = interquartile range, violin limits = lower and higher values. The asterisks over the violin plots indicate the statistical difference as determined by a pairwise Wilcoxon test. The black lines indicate the cell types that have been put in comparison. $^{**}p < 0.01$ and $^{***}p < 0.001$. Scale bars: 50 μm.

(F and G) Plant Ontology enrichment analysis of DEGs ($-0.6 \leq \log2FC \geq 0.6$, FDR ≤ 0.05, compared to the expression in the wild type) in *pMP::MP* (F) and *pMP::MP11ir* (G). The analysis was performed with the ShinyGo 0.80[57] webtool using the default configuration settings.

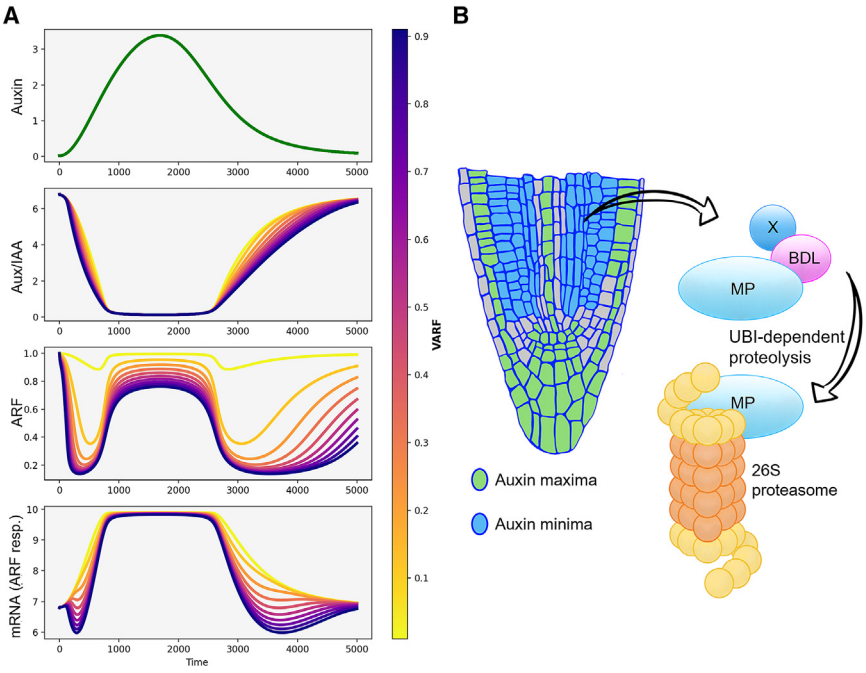

Figure 7. Conceptual investigation of the effect that Aux/IAA-mediated degradation of MP has on auxin signaling

(A) Modeling studies predict that altering the degradation of ARF relative to Aux/IAA sharpens signaling output. Graphs illustrate the outcome following a pulse of auxin of both the ARF gene itself and a hypothetical mRNA target. By increasing the parameter VARF (i.e., increasing the rate of ARF degradation in response to Aux/IAA) results in lower signaling output under low levels of auxin, but output rapidly rises under increasing auxin levels to produce a more switch-like response. As auxin levels decrease, auxin output falls more rapidly in simulations with higher values of VARF relative to those with lower values. However, the sharpness of the response to a reduction in auxin levels is not as steep as the response to an increase in auxin levels. Note that the initial condition is steady values without auxin. (B) Model of MP degradation mechanisms in region of auxin minima. The interaction of BDL with MP might recruit additional factors involved in the ubiquitin-dependent proteolysis, leading to MP proteasomal degradation. On the contrary, in root tissues characterized by high auxin, MP protein accumulates as it is uncoupled from the BDL interaction.

protein AFF1 can interact with ARF19 and ARF7 to trigger their ubiquitin-dependent degradation.[61]

Multiple factors likely act in MP post-translational regulation in addition to the one revealed in this work. For instance, SUMOylation has been shown to play a role in the regulation of ARF7 activity.[62] SUMOylation and ubiquitination can coexist to regulate protein degradation through the proteasome.[63,64] Interestingly, sequence analysis with the "GPS-SUMO" web server[65] revealed the presence of putative SUMOylation sites and SUMO-interaction motifs in the MP protein sequence (Table S1).

Other class A ARFs are post-translationally regulated by proteasomal degradation. Even though we did not observe significant changes in ARF6 and ARF8 accumulation upon proteasome inhibition, it has been reported that ARF6 and ARF8 levels are regulated by the proteasome during adventitious root development.[66] Moreover, it was shown that ARF7 and ARF19 nuclear-cytoplasmic partitioning is also regulated by controlled degradation.[61] Proteasomal degradation was reported to also be required for the regulation of a few repressor ARFs such as ARF1,[67] ARF2,[68] and ARF17,[66] suggesting a wider relevance of this process for the post-translational regulation of ARF proteins. It is possible that ARF regulation through degradation could be a conserved mechanism across evolution. Indeed, in *Marchantia polymorpha*, MpARF1 and MpARF2 proteasomal degradation regulates their stoichiometry and functionality.[69]

We show that the two MP isoforms differ not only in the patterns of protein accumulation but also in the way they mediate downstream responses to auxin. Mutant *mp* lines complemented with MP11ir are unresponsive to low levels of auxin in root elongation assays and showed more severe phenotypic defects. This indicates that the auxin responsiveness of the canonical MP isoform, represented by its stabilization under high auxin, is required to properly coordinate specific developmental processes, such as vasculature formation and columella cells organization. We believe that this activity involves the regulation of the spatial expression of target genes, which need to be activated only in a restricted subset of cells. Indeed, a higher number of MP direct targets were upregulated in MP11ir roots with respect to what was observed in canonical MP-expressing lines. According to this, canonical MP post-translational regulation might be required to maintain the proper expression of downstream genes.

From the analysis of previously published datasets, we could detect MP direct target gene[24] expression among 14 different root tissues (Figure S6D).[70] Only a few of these tissues, such as the xylem or the epidermis, have high auxin contents. Others, like the cortex, the endodermis, or the pericycle, have lower levels of auxin, implying that target gene activation in these tissues should require auxin-independent MP activity. We suggest that the MP11ir variant could cooperate for the expression of target genes at under-threshold auxin levels. We found six direct MP targets whose expression was reduced in *pMP::MP* but unaltered in *pMP::MP11ir* roots (Figure S6C). With the only exception of *ACL5*, which is expressed at low levels in the xylem, all the other genes have peak expression in the cortex, endodermis, endo-cortex, pericycle, root cap, and central stele,[41] suggesting that MP11ir could be important for their correct activation. Our hypothesis is that in wild-type roots, the two isoforms act in concert: the prevalent canonical isoform mediating a strong auxin-inducible activation of targets and MP11ir providing low-level activation of targets in a wider number of cells in an auxin-independent manner.

Although it is still unclear what the impact is of MP isoforms' auxin-mediated regulation on root development, the difference

between MP and MP11ir in target gene expression suggests that the two isoforms have non-redundant functions. Recently, it has been proposed that the formation of both AS isoforms is needed for somatic embryogenesis.[71] From an evolutive point of view, it has been shown that the event of intron retention associated with the generation of the MP11ir isoform is conserved across plant species, with an evolutionary depth that reaches the bryophyte.[72] This suggests that the mechanisms of regulation of *MP* described in this work are conserved and may have a biological relevance in many species.

Finally, by experimentation alone, it was not possible to disentangle the effect that the Aux/IAA-dependent degradation of MP would have on auxin output. We therefore generated a mathematical model of the auxin response to explore the effect that Aux/IAA-dependent degradation of MP would confer on auxin signaling. By altering the levels of Aux/IAA-dependent MP degradation in a range of simulations, we predicted sharper response kinetics in MP targets. In a dynamic system, this would allow changes in the auxin level to confer a more switch-like binary response to downstream genes expression.

In conclusion, our findings describe a level of regulation of MP, highlighting the importance of tissue-specific interplay between post-transcriptional and post-translational modifications to control auxin perception. In the last years, many non-canonical auxin signaling mechanisms have been discovered, revealing a high level of complexity.[73–75] Our work contributes to substantiate this vision, showing that the regulatory mechanisms of ARF activity and their cell/tissue specificity are much more complex than the canonical auxin paradigm, indicating the necessity for additional efforts to clarify how ARFs and Aux/IAAs cooperate in various developmental contexts to modulate auxin signaling and development.

Limitations of the study

Even though BDL has been shown to regulate MP degradation, the molecular mechanisms involved in this process have not been identified. Likewise, we could not demonstrate whether MP tissue-specific degradation is due to direct ubiquitination or SUMOylation.

Despite the phenotypical differences and changes in target expression observed in plants expressing only one of the isoforms, the specific functions of MP and MP11ir have not been elucidated yet.

RESOURCE AVAILABILITY

Lead contact

Additional information and request could be directed to the lead contact, Lucia Colombo (lucia.colombo@unimi.it).

Materials availability

Material newly produced in this work is available from the lead contact upon reasonable request.

Data and code availability

- RNA-seq raw data are available at the NCBI SRA database under the BioProject NCBI: PRJNA1165180.
- The Jupyter notebook describing the mathematical modeling code is available at Zenodo: https://doi.org/10.5281/zenodo.7716649.
- Any additional information required to re-analyze the data reported in this paper is available from the lead contact upon request.

ACKNOWLEDGMENTS

A.C. was founded by MIUR. M.C. and L.C. were supported by MIUR-PRIN 2022. J.T. was founded by an INRAE/University of Nottingham PhD grant. T.V. was founded by grant ANR-2014-CE11-0018. A.B. and E.C. were funded by Royal Society grants UF160729 and RGF/EA/180308. R.B. acknowledges a BBSRC Discovery Fellowship (BB/S011102/1). D.W. is funded by the European Research Council (ERC; AdG "DIRNDL"; 833867). J.M.M. was funded by a DFG grant (MU 4286/1-1). We thank Jason Banda for the help in the tissue-specific measurements of the fluorescent signals. A.C. thanks Rosanna Petrella, Cecilia Zumajo Cardona, and Chiara Mizzotti for the helpful suggestions. Part of this work was performed at NOLIMITS, an advanced imaging facility established by the Università degli Studi di Milano. The graphical abstract was generated with BioRender.

AUTHOR CONTRIBUTIONS

Conceived and designed the experiments, A.C., A.B., and L.C.; performed the experiments, A.C., C.A., J.T., M.C., E.C., and X.X.; contributed reagents/materials/analysis tools, A.B., L.C., K.K., M.J.B., T.V., and D.W.; analyzed the data, A.C., C.A., A.B., L.C., M.C., R.B., D.W., M.M.K., and J.M.M.; performed mathematical modeling, E.F.; wrote the paper, A.C., L.C., A.B., R.B., and M.M.K.

DECLARATION OF INTERESTS

The authors declare no competing interests.

STAR★METHODS

Detailed methods are provided in the online version of this paper and include the following:

- KEY RESOURCES TABLE
- EXPERIMENTAL MODEL AND STUDY PARTICIPANT DETAILS
  - Plant material and growth conditions
- METHOD DETAILS
  - Reporter lines generation
  - Polysome fraction extraction and RNA extraction
  - Auxin, bortezomib, MG132, PYR41 and DEX treatments
  - Confocal microscopy
  - Signal intensity measurements
  - Root morphology analysis
  - Root elongation assay
  - RNA sequencing and data analyses
  - Mathematical modeling
  - Ubiquitination and sumoylation sites prediction
- QUANTIFICATION AND STATISTICAL ANALYSIS

SUPPLEMENTAL INFORMATION

Supplemental information can be found online at https://doi.org/10.1016/j.celrep.2024.115083.

Received: May 3, 2024
Revised: September 26, 2024
Accepted: November 26, 2024
Published: December 15, 2024

REFERENCES

1. Weijers, D., and Wagner, D. (2016). Transcriptional Responses to the Auxin Hormone. Annu. Rev. Plant Biol. *67*, 539–574. https://doi.org/10.1146/annurev-arplant-043015-112122.

2. Li, S.-B., Xie, Z.-Z., Hu, C.-G., and Zhang, J.-Z. (2016). A Review of Auxin Response Factors (ARFs) in Plants. Front. Plant Sci. *7*, 47. https://doi.org/10.3389/fpls.2016.00047.

3. Rademacher, E.H., Möller, B., Lokerse, A.S., Llavata-Peris, C.I., Van Den Berg, W., and Weijers, D. (2011). A cellular expression map of the Arabidopsis AUXIN RESPONSE FACTOR gene family. Plant J. *68*, 597–606. https://doi.org/10.1111/j.1365-313X.2011.04710.x.

4. Okushima, Y., Overvoorde, P.J., Arima, K., Alonso, J.M., Chan, A., Chang, C., Ecker, J.R., Hughes, B., Lui, A., Nguyen, D., et al. (2005). Functional genomic analysis of the AUXIN RESPONSE FACTOR gene family members in Arabidopsis thaliana: Unique and overlapping functions of ARF7 and ARF19. Plant Cell *17*, 444–463. https://doi.org/10.1105/tpc.104.028316.

5. Rademacher, E.H., Lokerse, A.S., Schlereth, A., Llavata-Peris, C.I., Bayer, M., Kientz, M., FreireRios, A., Borst, J.W., Lukowitz, W., Jürgens, G., and Weijers, D. (2012). Different Auxin Response Machineries Control Distinct Cell Fates in the Early Plant Embryo. Dev. Cell *22*, 211–222. https://doi.org/10.1016/j.devcel.2011.10.026.

6. Boer, D.R., Freire-Rios, A., Van Den Berg, W.A.M., Saaki, T., Manfield, I.W., Kepinski, S., López-Vidrieo, I., Franco-Zorrilla, J.M., De Vries, S.C., Solano, R., et al. (2014). Structural basis for DNA binding specificity by the auxin-dependent ARF transcription factors. Cell *156*, 577–589. https://doi.org/10.1016/j.cell.2013.12.027.

7. Ulmasov, T., Hagen, G., and Guilfoyle, T.J. (1997). ARF1, a transcription factor that binds to auxin response elements. Science *276*, 1865–1868. https://doi.org/10.1126/science.276.5320.1865.

8. Tiwari, S.B., Hagen, G., and Guilfoyle, T. (2003). The Roles of Auxin Response Factor Domains in Auxin-Responsive Transcription. Plant Cell *15*, 533–543. https://doi.org/10.1105/tpc.008417.

9. Roosjen, M., Paque, S., and Weijers, D. (2018). Auxin Response Factors: Output control in auxin biology. J. Exp. Bot. *69*, 179–188. https://doi.org/10.1093/jxb/erx237.

10. Guilfoyle, T.J. (2015). The PB1 domain in auxin response factor and aux/IAA proteins: A versatile protein interaction module in the auxin response. Plant Cell *27*, 33–43. https://doi.org/10.1105/tpc.114.132753.

11. Nanao, M.H., Vinos-Poyo, T., Brunoud, G., Thévenon, E., Mazzoleni, M., Mast, D., Lainé, S., Wang, S., Hagen, G., Li, H., et al. (2014). Structural basis for oligomerization of auxin transcriptional regulators. Nat. Commun. *5*, 3617. https://doi.org/10.1038/ncomms4617.

12. Vernoux, T., Brunoud, G., Farcot, E., Morin, V., Van Den Daele, H., Legrand, J., Oliva, M., Das, P., Larrieu, A., Wells, D., et al. (2011). The auxin signalling network translates dynamic input into robust patterning at the shoot apex. Mol. Syst. Biol. *7*, 508. https://doi.org/10.1038/msb.2011.39.

13. Tiwari, S.B., Hagen, G., and Guilfoyle, T.J. (2004). Aux/IAA Proteins Contain a Potent Transcriptional Repression Domain. Plant Cell *16*, 533–543. https://doi.org/10.1105/tpc.017384.

14. Ulmasov, T., Murfett, J., Hagen, G., and Guilfoyle, T.J. (1997). Aux/IAA Proteins Repress Expression of Reporter Genes Containing Natural and Highly Active Synthetic Auxin Response Elements. Society *9*, 1963–1971. https://doi.org/10.1105/tpc.9.11.1963.

15. Szemenyei, H., Hannon, M., and Long, J.A. (2008). TOPLESS mediates auxin-dependent transcriptional repression during Arabidopsis embryogenesis. Science *319*, 1384–1386. https://doi.org/10.1126/science.1151461.

16. Wang, L., Kim, J., and Somers, D.E. (2013). Transcriptional corepressor TOPLESS complexes with pseudoresponse regulator proteins and histone deacetylases to regulate circadian transcription. Proc. Natl. Acad. Sci. USA *110*, 761–766. https://doi.org/10.1073/pnas.1215010110.

17. Wu, M.F., Yamaguchi, N., Xiao, J., Bargmann, B., Estelle, M., Sang, Y., and Wagner, D. (2015). Auxin-regulated chromatin switch directs acquisition of flower primordium founder fate. Elife *4*, e09269. https://doi.org/10.7554/eLife.09269.

18. Piya, S., Shrestha, S.K., Binder, B., Stewart, C.N., Jr., and Hewezi, T. (2014). Protein-protein interaction and gene co-expression maps of ARFs and Aux/IAAs in Arabidopsis. Front. Plant Sci. *5*, 744–749. https://doi.org/10.3389/fpls.2014.00744.

19. Dharmasiri, N., Dharmasiri, S., and Estelle, M. (2005). The F-box protein TIR1 is an auxin receptor. Nature *435*, 441–445. https://doi.org/10.1038/nature03543.

20. Kepinski, S., and Leyser, O. (2005). The Arabidopsis F-box protein TIR1 is an auxin receptor. Nature *435*, 446–451. https://doi.org/10.1038/nature03542.

21. Tan, X., Calderon-Villalobos, L.I.A., Sharon, M., Zheng, C., Robinson, C.V., Estelle, M., and Zheng, N. (2007). Mechanism of auxin perception by the TIR1 ubiquitin ligase. Nature *446*, 640–645. https://doi.org/10.1038/nature05731.

22. Reed, J.W. (2001). Roles and activities of Aux/IAA proteins in Arabidopsis. Trends Plant Sci. *6*, 420–425. https://doi.org/10.1016/S1360-1385(01)02042-8.

23. Berleth, T., and Jürgens, G. (1993). The role of the monopteros gene in organising the basal body region of the Arabidopsis embryos. Trends Genet. *9*, 299. https://doi.org/10.1016/0168-9525(93)90246-E.

24. Schlereth, A., Möller, B., Liu, W., Kientz, M., Flipse, J., Rademacher, E.H., Schmid, M., Jürgens, G., and Weijers, D. (2010). MONOPTEROS controls embryonic root initiation by regulating a mobile transcription factor. Nature *464*, 913–916. https://doi.org/10.1038/nature08836.

25. Hardtke, C.S., and Berleth, T. (1998). The *Arabidopsis* gene *MONOPTEROS* encodes a transcription factor mediating embryo axis formation and vascular development. EMBO J. *17*, 1405–1411. https://doi.org/10.1093/emboj/17.5.1405.

26. Weijers, D., Schlereth, A., Ehrismann, J.S., Schwank, G., Kientz, M., and Jürgens, G. (2006). Auxin triggers transient local signaling for cell specification in Arabidopsis embryogenesis. Dev. Cell *10*, 265–270. https://doi.org/10.1016/j.devcel.2005.12.001.

27. De Smet, I., Lau, S., Voß, U., Vanneste, S., Benjamins, R., Rademacher, E.H., Schlereth, A., De Rybel, B., Vassileva, V., Grunewald, W., et al. (2010). Bimodular auxin response controls organogenesis in Arabidopsis. Proc. Natl. Acad. Sci. USA *107*, 2705–2710. https://doi.org/10.1073/pnas.0915001107.

28. Krogan, N.T., Marcos, D., Weiner, A.I., and Berleth, T. (2016). The auxin response factor MONOPTEROS controls meristem function and organogenesis in both the shoot and root through the direct regulation of PIN genes. New Phytol. *212*, 42–50. https://doi.org/10.1111/nph.14107.

29. Donner, T.J., Sherr, I., and Scarpella, E. (2009). Regulation of preprocambial cell state acquisition by auxin signaling in Arabidopsis leaves. Development *136*, 3235–3246. https://doi.org/10.1242/dev.037028.

30. Chung, Y., Zhu, Y., Wu, M.F., Simonini, S., Kuhn, A., Armenta-Medina, A., Jin, R., Østergaard, L., Gillmor, C.S., and Wagner, D. (2019). Auxin Response Factors promote organogenesis by chromatin-mediated repression of the pluripotency gene SHOOTMERISTEMLESS. Nat. Commun. *10*, 886. https://doi.org/10.1038/s41467-019-08861-3.

31. Yamaguchi, N., Wu, M.F., Winter, C.M., Berns, M.C., Nole-Wilson, S., Yamaguchi, A., Coupland, G., Krizek, B.A., and Wagner, D. (2013). A Molecular Framework for Auxin-Mediated Initiation of Flower Primordia. Dev. Cell *24*, 271–282. https://doi.org/10.1016/j.devcel.2012.12.017.

32. Yamaguchi, N., Jeong, C.W., Nole-Wilson, S., Krizek, B.A., and Wagner, D. (2016). AINTEGUMENTA and AINTEGUMENTA-LIKE6/PLETHORA3 Induce LEAFY expression in response to auxin to promote the onset of flower formation in arabidopsis1[OPEN]. Plant Physiol. *170*, 283–293. https://doi.org/10.1104/pp.15.00969.

33. Galbiati, F., Sinha Roy, D., Simonini, S., Cucinotta, M., Ceccato, L., Cuesta, C., Simaskova, M., Benkova, E., Kamiuchi, Y., Aida, M., et al. (2013). An integrative model of the control of ovule primordia formation. Plant J. *76*, 446–455. https://doi.org/10.1111/tpj.12309.

34. Cucinotta, M., Cavalleri, A., Guazzotti, A., Astori, C., Manrique, S., Bombarely, A., Oliveto, S., Biffo, S., Weijers, D., Kater, M.M., and Colombo, L. (2021). Alternative Splicing Generates a MONOPTEROS Isoform Required for Ovule Development. Curr. Biol. *31*, 892–899.e3. https://doi.org/10.1016/j.cub.2020.11.026.

35. Hamann, T., Benkova, E., Bäurle, I., Kientz, M., and Jürgens, G. (2002). Gene Encodes an Auxin Response Protein Inhibiting Embryo Patterning. Genes Dev. *16*, 1610–1615. https://doi.org/10.1101/gad.229402.clonal.

36. Khosla, A., Rodriguez-Furlan, C., Kapoor, S., Van Norman, J.M., and Nelson, D.C. (2020). A series of dual-reporter vectors for ratiometric analysis of protein abundance in plants. Plant Direct *4*, e002311. https://doi.org/10.1002/pld3.231.

37. Trichas, G., Begbie, J., and Srinivas, S. (2008). Use of the viral 2A peptide for bicistronic expression in transgenic mice. BMC Biol. *6*, 40. https://doi.org/10.1186/1741-7007-6-40.

38. Truskina, J., Han, J., Chrysanthou, E., Galvan-ampudia, C.S., Lainé, S., Brunoud, G., Macé, J., Bellows, S., Legrand, J., Bågman, A.M., et al. (2021). A network of transcriptional repressors modulates auxin responses. Nature *589*, 116–119. https://doi.org/10.1038/s41586-020-2940-2.

39. Dastidar, M.G., Scarpa, A., Mägele, I., Ruiz-Duarte, P., von Born, P., Bald, L., Jouannet, V., and Maizel, A. (2019). ARF5/MONOPTEROS directly regulates miR390 expression in the Arabidopsis thaliana primary root meristem. Plant Direct *3*. https://doi.org/10.1002/pld3.116.

40. Doronina, V.A., Wu, C., de Felipe, P., Sachs, M.S., Ryan, M.D., and Brown, J.D. (2008). Site-Specific Release of Nascent Chains from Ribosomes at a Sense Codon. Mol. Cell Biol. *28*, 4227–4239. https://doi.org/10.1128/mcb.00421-08.

41. Ryu, K.H., Huang, L., Kang, H.M., and Schiefelbein, J. (2019). Single-cell RNA sequencing resolves molecular relationships among individual plant cells. Plant Physiol. *179*, 1444–1456. https://doi.org/10.1104/pp.18.01482.

42. Liao, C.Y., Smet, W., Brunoud, G., Yoshida, S., Vernoux, T., and Weijers, D. (2015). Reporters for sensitive and quantitative measurement of auxin response. Nat. Methods *12*, 207–210. https://doi.org/10.1038/nmeth.3279.

43. Band, L.R., Wells, D.M., Fozard, J.A., Ghetiu, T., French, A.P., Pound, M.P., Wilson, M.H., Yu, L., Li, W., Hijazi, H.I., et al. (2014). Systems analysis of auxin transport in the Arabidopsis root apex. Plant Cell *26*, 862–875. https://doi.org/10.1105/tpc.113.119495.

44. Lewis, D.R., Negi, S., Sukumar, P., and Muday, G.K. (2011). Ethylene inhibits lateral root development, increases IAA transport and expression of PIN3 and PIN7 auxin efflux carriers. Development *138*, 3485–3495. https://doi.org/10.1242/dev.065102.

45. Brunoud, G., Wells, D.M., Oliva, M., Larrieu, A., Mirabet, V., Burrow, A.H., Beeckman, T., Kepinski, S., Traas, J., Bennett, M.J., and Vernoux, T. (2012). A novel sensor to map auxin response and distribution at high spatio-temporal resolution. Nature *482*, 103–106. https://doi.org/10.1038/nature10791.

46. De Smet, I., Vanneste, S., Inzé, D., and Beeckman, T. (2006). Lateral root initiation or the birth of a new meristem. Plant Mol. Biol. *60*, 871–887. https://doi.org/10.1007/s11103-005-4547-2.

47. Benková, E., Michniewicz, M., Sauer, M., Teichmann, T., Seifertová, D., Jürgens, G., and Friml, J. (2003). Local, Efflux-Dependent Auxin Gradients as a Common Module for Plant Organ Formation. Cell *115*, 591–602. https://doi.org/10.1016/S0092-8674(03)00924-3.

48. Gladman, N.P., Marshall, R.S., Lee, K.H., and Vierstra, R.D. (2016). The proteasome stress regulon is controlled by a pair of NAC transcription factors in arabidopsis. Plant Cell *28*, 1279–1296. https://doi.org/10.1105/tpc.15.01022.

49. Chen, D., Frezza, M., Schmitt, S., Kanwar, J., and Dou, Q.P. (2011). Bortezomib as the First Proteasome Inhibitor Anticancer Drug: Current Status and Future Perspectives. Curr. Cancer Drug Targets *11*, 239–253. https://doi.org/10.2174/156800911794519752.

50. Kisselev, A.F., and Goldberg, A.L. (2001). Proteasome inhibitors: From research tools to drug candidates. Chem. Biol. *8*, 739–758. https://doi.org/10.1016/S1074-5521(01)00056-4.

51. Chen, C., Meng, Y., Wang, L., Wang, H.X., Tian, C., Pang, G.D., Li, H.H., and Du, J. (2014). Ubiquitin-activating enzyme E1 inhibitor PYR41 attenuates angiotensin II-induced activation of dendritic cells via the IκBa/NF-κB and MKP1/ERK/STAT1 pathways. Immunology *142*, 307–319. https://doi.org/10.1111/imm.12255.

52. Li, Y., Sun, D., Ma, Z., Yamaguchi, K., Wang, L., Zhong, S., Yan, X., Shang, B., Nagashima, Y., Koiwa, H., et al. (2020). Degradation of SERRATE via ubiquitin-independent 20S proteasome to survey RNA metabolism. Nat. Plants *6*, 970–982. https://doi.org/10.1038/s41477-020-0721-4.

53. Qiu, W., Xu, C., Xiao, X., and Xu, D. (2019). Computational Prediction of Ubiquitination Proteins Using Evolutionary Profiles and Functional Domain Annotation. Curr. Genom. *20*, 389–399. https://doi.org/10.2174/1389202919666191014091250.

54. Chandler, J.W. (2016). Auxin response factors. Plant Cell Environ. *39*, 1014–1028. https://doi.org/10.1111/pce.12662.

55. Hamann, T., Mayer, U., and Jürgens, G. (1999). The auxin-insensitive bodenlos mutation affects primary root formation and apical-basal patterning in the Arabidopsis embryo. Development *1395*, 1387–1395.

56. Yang, J.H., and Wang, H. (2016). Molecular mechanisms for vascular development and secondary cell wall formation. Front. Plant Sci. *7*, 356–358. https://doi.org/10.3389/fpls.2016.00356.

57. Ge, S.X., Jung, D., Yao, R., and Yao, R. (2020). ShinyGO: A graphical gene-set enrichment tool for animals and plants. Bioinformatics *36*, 2628–2629. https://doi.org/10.1093/bioinformatics/btz931.

58. Farcot, E., Lavedrine, C., and Vernoux, T. (2015). A modular analysis of the auxin signalling network. PLoS One *10*, 01222311–e122326. https://doi.org/10.1371/journal.pone.0122231.

59. Luo, J., Zhou, J.J., and Zhang, J.Z. (2018). Aux/IAA gene family in plants: Molecular structure, regulation, and function. Int. J. Mol. Sci. *19*, 259. https://doi.org/10.3390/ijms19010259.

60. Song, G., Olatunji, D., Montes, C., Clark, N.M., Pu, Y., Kelley, D.R., and Walley, J.W. (2021). Quantitative proteomics reveals extensive lysine ubiquitination in the Arabidopsis root proteome and uncovers novel transcription factor stability states. Preprint at bioRxiv. https://doi.org/10.1101/2021.01.07.425780.

61. Jing, H., Korasick, D.A., Emenecker, R.J., Morffy, N., Wilkinson, E.G., Powers, S.K., and Strader, L.C. (2022). Regulation of AUXIN RESPONSE FACTOR condensation and nucleo-cytoplasmic partitioning. Nat. Commun. *13*, 4015–4111. https://doi.org/10.1038/s41467-022-31628-2.

62. Orosa-Puente, B., Leftley, N., von Wangenheim, D., Banda, J., Srivastava, A.K., Hill, K., Truskina, J., Bhosale, R., Morris, E., Srivastava, M., et al. (2018). Root branching toward water involves posttranslational modification of transcription factor ARF7. Science *362*, 1407–1410. https://doi.org/10.1126/science.aau3956.

63. Miteva, M., Keusekotten, K., Hofmann, K., Praefcke, G.J.K., and Dohmen, R.J. (2010). Sumoylation as a signal for polyubiquitylation and proteasomal degradation. Subcell. Biochemist *54*, 195–214. https://doi.org/10.1007/978-1-4419-6676-6_16.

64. Gill, G. (2004). SUMO and ubiquitin in the nucleus: Different functions, similar mechanisms? Genes Dev. *18*, 2046–2059. https://doi.org/10.1101/gad.1214604.

65. Zhao, Q., Xie, Y., Zheng, Y., Jiang, S., Liu, W., Mu, W., Liu, Z., Zhao, Y., Xue, Y., and Ren, J. (2014). GPS-SUMO : a tool for the prediction of sumoylation sites and SUMO-interaction motifs. Nucleic Acids Res. *42*, W325–W330. https://doi.org/10.1093/nar/gku383.

66. Lakehal, A., Chaabouni, S., Cavel, E., Le Hir, R., Ranjan, A., Raneshan, Z., Novák, O., Păcurar, D.I., Perrone, I., Jobert, F., et al. (2019). A Molecular

Framework for the Control of Adventitious Rooting by TIR1/AFB2-Aux/IAA-Dependent Auxin Signaling in Arabidopsis. Mol. Plant *12*, 1499–1514. https://doi.org/10.1016/j.molp.2019.09.001.

67. Salmon, J., Ramos, J., and Callis, J. (2008). Degradation of the auxin response factor ARF1. Plant J. *54*, 118–128. https://doi.org/10.1111/j.1365-313X.2007.03396.x.
68. Li, H., Johnson, P., Stepanova, A., Alonso, J.M., and Ecker, J.R. (2004). Convergence of signaling pathways in the control of differential cell growth in Arabidopsis. Dev. Cell *7*, 193–204. https://doi.org/10.1016/j.devcel.2004.07.002.
69. Das, S., de Roij, M., Bellows, S., Kohlen, W., Farcot, E., Weijers, D., and Borst, J.W. (2022). Selective degradation of ARF monomers controls auxin response in Marchantia. Preprint at bioRxiv, 515187. https://doi.org/10.1101/2022.11.04.515187.
70. Brady, S.M., Orlando, D.A., Lee, J.-Y., Wang, J.Y., Koch, J., Dinneny, J.R., Mace, D., Ohler, U., and Benfey, P.N. (2007). Dominant Expression Patterns. Science *318*, 801–806.
71. Wójcikowska1, B., Belaidi1, S., Mironova, V., and Boisivon, H.R. (2024). MONOPTEROS isoform MP11ir role during somatic embryogenesis in Arabidopsis thaliana. Preprint at bioRxiv. https://doi.org/10.1101/2024.07.17.603838.
72. Timofeyenko, K., Kanavalau, D., Alexiou, P., Kalyna, M., and Růžička, K. (2023). Catsnap: a user-friendly algorithm for determining the conservation of protein variants reveals extensive parallelisms in the evolution of alternative splicing. New Phytol. *238*, 1722–1732. https://doi.org/10.1111/nph.18799.
73. Simonini, S., Deb, J., Moubayidin, L., Stephenson, P., Valluru, M., Freire-Rios, A., Sorefan, K., Weijers, D., Friml, J., and Østergaard, L. (2016). A noncanonical auxin-sensing mechanism is required for organ morphogenesis in arabidopsis. Genes Dev. *30*, 2286–2296. https://doi.org/10.1101/gad.285361.116.
74. Kuhn, A., Harborough, S.R., McLaughlin, H.M., Natarajan, B., Verstraeten, I., Friml, J., Kepinski, S., and Østergaard, L. (2020). Direct ETTIN-auxin interaction controls chromatin states in gynoecium development. Elife *9*, 1–18. https://doi.org/10.7554/eLife.51787.
75. McLaughlin, H.M., Ang, A.C.H., and Østergaard, L. (2021). Noncanonical Auxin Signaling. Cold Spring Harbor Perspect. Biol. *13*, a039917. https://doi.org/10.1101/cshperspect.a039917.
76. Schindelin, J., Arganda-Carreras, I., Frise, E., Kaynig, V., Longair, M., Pietzsch, T., Preibisch, S., Rueden, C., Saalfeld, S., Schmid, B., et al. (2012). Fiji: An open-source platform for biological-image analysis. Nat. Methods *9*, 676–682. https://doi.org/10.1038/nmeth.2019.
77. Legland, D., Arganda-Carreras, I., and Andrey, P. (2016). MorphoLibJ: Integrated library and plugins for mathematical morphology with ImageJ. Bioinformatics *32*, 3532–3534. https://doi.org/10.1093/bioinformatics/btw413.
78. Bolger, A.M., Lohse, M., and Usadel, B. (2014). Trimmomatic: A flexible trimmer for Illumina sequence data. Bioinformatics *30*, 2114–2120. https://doi.org/10.1093/bioinformatics/btu170.
79. Dobin, A., Davis, C.A., Schlesinger, F., Drenkow, J., Zaleski, C., Jha, S., Batut, P., Chaisson, M., and Gingeras, T.R. (2013). STAR: ultrafast universal RNA-seq aligner. Bioinformatics *29*, 15–21. https://doi.org/10.1093/bioinformatics/bts635.
80. Liao, Y., Smyth, G.K., and Shi, W. (2014). FeatureCounts: An efficient general purpose program for assigning sequence reads to genomic features. Bioinformatics *30*, 923–930. https://doi.org/10.1093/bioinformatics/btt656.
81. Love, M.I., Huber, W., and Anders, S. (2014). Moderated estimation of fold change and dispersion for RNA-seq data with DESeq2. Genome Biol. *15*, 550–621. https://doi.org/10.1186/s13059-014-0550-8.
82. Weijers, D., Benkova, E., Jäger, K.E., Schlereth, A., Hamann, T., Kientz, M., Wilmoth, J.C., Reed, J.W., and Jürgens, G. (2005). Developmental specificity of auxin response by pairs of ARF and Aux/IAA transcriptional regulators. EMBO J. *24*, 1874–1885. https://doi.org/10.1038/sj.emboj.7600659.
83. Oliveto, S., Alfieri, R., Miluzio, A., Scagliola, A., Secli, R.S., Gasparini, P., Grosso, S., Cascione, L., Mutti, L., and Biffo, S. (2018). A polysome-based microRNA screen identifies miR-24-3p as a novel promigratory miRNA in mesothelioma. Cancer Res. *78*, 5741–5753. https://doi.org/10.1158/0008-5472.CAN-18-0655.
84. Serna, A., Marcotegui, B., Decencière, E., Baldeweck, T., Pena, A.M., and Brizion, S. (2014). Segmentation of elongated objects using attribute profiles and area stability: Application to melanocyte segmentation in engineered skin. Pattern Recogn. Lett. *47*, 172–182. https://doi.org/10.1016/j.patrec.2014.03.014.
85. Vaughan-Hirsch, J., Tallerday, E.J., Burr, C.A., Hodgens, C., Boeshore, S.L., Beaver, K., Melling, A., Sari, K., Kerr, I.D., Šimura, J., et al. (2021). Function of the pseudo phosphotransfer proteins has diverged between rice and Arabidopsis. Plant J. *106*, 159–173. https://doi.org/10.1111/tpj.15156.

STAR★METHODS

KEY RESOURCES TABLE

REAGENT or RESOURCE	SOURCE	IDENTIFIER
Bacterial and virus strains		
Agrobacterium tumefaciens C58pMP90 strain	Widely distributed	N/A
Agrobacterium tumefaciens GV3101 strain	Widely distributed	N/A
Chemicals, peptides, and recombinant proteins		
Indole-3-acetic acid	Merck	Cat#87-51-4
Bortezomib	Merck	Cat#179324-69-7
MG-132	Merck	Cat#133407-82-6
PYR-41	Merck	Cat#418805-02-4
Dexamethasone	Merck	Cat#50-02-2
Propidium iodide	Merck	Cat#25535-16-4
Renaissance SR2200	Renaissance Chemicals	SR2200
DMSO	Merck	Cat#67-68-5
MS medium	Duchefa Biochemie	Cat#M0221
Cycloheximide	Merck	Cat#66-81-9
Chloramphenicol	Merck	Cat#56-75-7
Glycerol	Merck	Cat#56-81-5
Critical commercial assays		
Q5 High-Fidelity DNA Polymerase	NEB	Cat#M0491S
GoTaq DNA Polymerase	Promega	Cat#M3001
SuperScriptTM IV VILOTM Master Mix with ezDNaseTM	ThermoFisher Scientific	Cat#11766050
iScript™ gDNA Clear cDNA Synthesis Kit	BIO-RAD	Cat#1725035
iTaq SYBR green master mix	BIO-RAD	Cat#1725121
Deposited data		
mathematical modeling code Jupyter notebook	This study	Zenodo: https://doi.org/10.5281/zenodo.7716649
RNA-SEQ raw reads	This study	NCBI: PRJNA1165180
Root single-cell RNA sequencing	Ryu et al.[41]	N/A
Root tissues transcriptomes	Brady et al.[70]	N/A
Experimental models: Organisms/strains		
Arabidopsis thaliana Col-0	The Nottingham Arabidopsis Stock Center (NASC)	N/A
Arabidopsis thaliana: pMP::MP:eGFP(mr)	Schlereth et al.[24]	N/A
Arabidopsis thaliana: pMP::MP:VENUS-2Ap-mTURQUOISE	This study	N/A
Arabidopsis thaliana: pMP:MP-GFP(ct)	This study	N/A
Arabidopsis thaliana: pARF6:ARF6:VENUS-2Ap-mTURQUOISE	This study	N/A
Arabidopsis thaliana: pARF8:ARF8:VENUS-2Ap-mTURQUOISE	This study	N/A
Arabidopsis thaliana: R2D2	Liao et al.[42]	N/A
Arabidopsis thaliana: GR:bdl	Weijers et al.[26]	N/A
Arabidopsis thaliana: pMP::MP	Cucinotta et al.[34]	N/A
Arabidopsis thaliana: pMP::MP11ir	Cucinotta et al.[34]	N/A

(*Continued on next page*)

Continued

REAGENT or RESOURCE	SOURCE	IDENTIFIER
Oligonucleotides		
Primers	this study	Table S6
Recombinant DNA		
pMP::MP:VENUS-2Ap-mTURQUOISE	This study	N/A
pARF6:ARF6:VENUS-2Ap-mTURQUOISE	This study	N/A
pARF8:ARF8:VENUS-2Ap-mTURQUOISE	This study	N/A
pMP:MP-GFP(ct)	This study	N/A
Software and algorithms		
LAS X	Leica	www.leica-microsystems.com
NIS-Elements	Nikon	www.microscope.healthcare.nikon.com
BioLogic LP software	BIO-RAD	www.bio-rad.com
CFX Maestro	BIO-RAD	www.bio-rad.com
Fiji	Schindelin et al.[76]	N/A
MorphoLibJ plugin	Legland et al.[77]	N/A
Trimmomatic (v.0.36)	Bolger et al.[78]	N/A
STAR (v2.7.10a)	Dobin et al.[79]	N/A
featureCounts (v2.0.1)	Liao et al.[80]	N/A
R (v4.3.3)	The R Project for Statistical Computing	https://www.r-project.org/
ShinyGo (v0.80)	Ge et al.[57]	http://bioinformatics.sdstate.edu/go/
Deseq2	Love et al.[81]	N/A

EXPERIMENTAL MODEL AND STUDY PARTICIPANT DETAILS

Plant material and growth conditions

Arabidopsis thaliana plants were grown in controlled conditions under long-day photoperiod (16h light, 8h dark) at 22°C. The *R2D2*[42] reporter lines, the *pMP::MP:EGFP(mr)*[24] reporter line, the GR:*bdl* inducible line[26] and *pMP::MP* and *pMP::MP11ir* complementation lines[34] were previously described. *pMP::MP:VENUS-2Ap-mTURQUOISE, pMP::MP:EGFP(mr),* p*MP:MP:EGFP(ct), pARF6::ARF6:VENUS-2Ap-mTURQUOISE, pARF8::ARF8:VENUS-2Ap-mTURQUOISE, R2D2*, GR:*bdl/pMP::MP:VENUS-2Ap-nlsmTURQUOISE,* GR:*bdl/R2D2,* wild type, *pMP::MP* and *pMP*::*MP11ir* seeds were sterilised with a solution of Triton 0.1%, commercial bleach 10%. After sterilisation, seeds were sown on half-strength MS medium and left at 4°C in the dark for 16h for stratification. Subsequentially, plates were transferred in growing chambers. All experiments have been performed using plants taken 5 days after the germination.

METHOD DETAILS

Reporter lines generation

The reporter lines *pMP::MP:VENUS-2Ap-mTURQUOISE*, *pARF6::ARF6:VENUS-2Ap-mTURQUOISE* and *pARF8::ARF8:VENUS-2Ap-mTURQUOISE* were generated by amplifying genomic DNA fragments containing regulatory regions upstream of the start codon and the coding region up to but not including the stop codon. For the generation of the reporter lines *pMP::MP:VENUS-2Ap-mTURQUOISE*, *pARF6::ARF6:VENUS-2Ap-mTURQUOISE* and *pARF8::ARF8:VENUS-2Ap-mTURQUOISE* the fragments amplified were for *MP* from −5418 bp, for *ARF6* from −3255 bp and for *ARF8* from −5091 bp. The resulting genomic DNA fragments were inserted into pDONR P4-P1R and recombined using Gateway recombination with a *mVENUS* pDONR211 plasmid (containing the full *mVENUS* sequence) and 2aP- *mTURQUOISE2* pDONR P2R-P3 plasmid (containing the sequence encoding the 2a peptide followed by the sequence of *mTURQUOISE2* with a nuclear-localization signal) into the pK7m34GW destination vector. The constructs were transformed into the Agrobacterium tumefaciens C58pMP90 strain using electroporation and then transformed into Col-0 plants by the floral dip method.

The C-terminal MP-GFP fusion was generated by amplifying stretches of the genomic *MP* sequence by PCR and introducing them into the pGreeenIIBASTA:NOSt vector in the following order: (1) 896 bp of the 3′UTR. (2) 3′ region of the coding sequence containing exons and introns. (3) 5′ region of the coding sequence containing exons and introns. (4) 4113 bp of the MP promoter upstream of the

ATG. This resulted in an MP cassette with a XhoI restriction site directly upstream of the ATG, an EcoRI restriction site in the coding sequence (that encodes the variable middle region of ARF proteins), and an SpeI restriction site directly upstream of the stop codon. Subsequently, PCR-amplified *EGFP* was inserted in SpeI restriction sites. The construct was transformed into *mp-B4149* heterozygous plants[82] by floral dip using the Agrobacterium strain GV3101(pSoup). Complementation of the rootless mp phenotype was confirmed in segregating T2 generation seedlings. No rootless individuals were found among PPT-resistant progeny of 3 independent lines segregating the *mp-B4149* mutation.

Primers are listed in Table S6.

Polysome fraction extraction and RNA extraction

Five days after germination wild-type Col-0 seedlings were used for polysomes isolation, accordingly to the protocol reported in.[34,83] 15%–50% Sucrose gradients, with or without 10 mmol/L EDTA, were added with the cell lysate and centrifuged at 39,000 rpm for 3 h in a SW41Ti Beckman rotor at 4°C. EDTA adjunct to the gradient and to the cell lysate leads to the disruption of polysomes complexes, allowing the discrimination of mRNA associated to translation complexes to the ones that precipitates at a certain density due to their molecular weight. After centrifugation, the absorbance of gradients at 254 nm were recorded continuously by BioLogic LP software (Bio-Rad), allowing the identification of three different translational complexes: (I) monosome, (II) light polysomes and (III) heavy polysomes. RNA was extracted from different fractions and quantified. The same quantity of RNA per each fraction was subsequentially used to generate cDNA with the SuperScript IV VILO Master Mix with ezDNase system (Invitrogen). The distribution of mRNAs among fractions was evaluated by RT-qPCR using a CFX96 thermocycler. Primers used are listed in Table S6.

Auxin, bortezomib, MG132, PYR41 and DEX treatments

Treatments were performed transferring seedlings 5 days after germination from plates to liquid half-strength MS, supplemented with either a mock solution or with the compound of interest. After an incubation time of 4h in the same growing condition, roots were imaged using confocal microscopy. Auxin treatments were performed using a final concentration of IAA in the medium of 1μM or adding the same volume of DMSO in the mock condition. Bortezomib, MG132 and PYR41 treatments were performed with a final concentration of 50 μM in the medium respectively, or with the same volume of DMSO in the mock sample. The dexamethasone induction of *GR:bdl* fusion protein was performed with a final concentration of 10 μM DEX, using DMSO as mock solution. DEX PYR41 double treatment has been performed with a final concentration of 10 μM DEX, 50 μM PYR41.

Confocal microscopy

For confocal laser scanning microscopy, roots were detached from seedlings and mounted in a solution of 10% glycerol, 10 μg/mL propidium iodide. R2D2 roots were mounted in a solution of 10% glycerol, 10 μg/mL Reinassance2200. For ovules and embryo imaging, pistils and young siliques were dissected and mounted in 10% glycerol. Samples were analyzed immediately after slides were prepared. The analysis of *pMP::MP:VENUS-2Ap-mTURQUOISE, pMP::MP:eGFP(mr),* p*MP:MP-GFP(ct), pARF6::ARF6:VENUS-2Ap-mTURQUOISE, pARF8::ARF8:VENUS-2Ap-mTURQUOISE* reporter lines in RAM, LRs primordia and ovules, as well as auxin treatments, was performed using a Leica TCS-SP5 confocal microscope. Bortezomib treatments have been imaged using a TCS-SP8 confocal microscope. R2D2 reporter line imaging, treatments with MG132, PYR41 and DEX, DEX/PYR41 have been imaged using a NIKON A1 confocal microscope. In all case, propidium iodide was excited at 514nm and detected at 610-650nm, VENUS was excited at 514nm and detected at 530–550nm. mTURQUOISE was excited at 405 nm and detected at 470-480nm. EGFP was excited at 488 nm and detected at 520-540nm. Reinassance 2200 was excited at 405nm and detected at 440-470nm. tdTOMATO was exited at 514nm and detected at 571-630nm. Images were collected in multi-channel mode with sequential settings in order to avoid emission signals crosstalk. In all cases, laser power, gain and pinhole size were set on control samples. Overlay images were generated using the Fiji ImageJ software.[76]

Signal intensity measurements

Signal intensity measurements were performed using the Fiji ImageJ software. For ratio-metric measurements of VENUS and mTURQUOISE signals in *pMP::MP:VENUS-2Ap-mTURQUOISE, pARF6::ARF6:VENUS-2Ap-mTURQUOISE* and *pARF8::ARF8:VENUS-2Ap-mTURQUOISE* reporter lines, the mTURQUOISE channel was used to obtain a binary mask highlighting all the nuclei with the reporter expression through automatic thresholding. Nuclei belonging to each different tissue analyzed were included manually in the ROI and automatically identified by the particle analyser (considering particles with an area bigger than 10 μm^2). VENUS and mTURQUOISE signal intensity was subsequently measured in all the individual nuclei identified. For the analysis of the R2D2 reporter, as well as the R2D2 signal upon GR:bdl DEX induction, the mDII-dTOMATO channel was used to generate the binary mask and in the identification of the single nuclei of the different tissues. In each nucleus identified, tdTOMATO and VENUS signals were measured subsequentially. For signals measurements in auxin, BTZ, MG132 and PYR41 treatments for each root the propidium iodide channel, showing the cellular organisation, has been used to describe a ROI to measure the mean gray value in mTQ and VENUS channels. Since in these cases the major changes observed were associated to RAM vascular cylinder, the ROI considered for further measurements was identified in the central stele including the endodermis, above the QC up and to a height corresponding to 25 cortical cells. For signals measurements in auxin and BTZ treatments on *pARF6::ARF6:VENUS-2Ap-mTURQUOISE* and

pARF8::ARF8:VENUS-2Ap-mTURQUOISE reporters, as well as in DEX and DEX/PYR41 treatments, the whole RAM up to a zone represented by 25 cortical cells has been considered for the analysis. The propidium iodide channel has been used for ROIs description also in these cases.

Root morphology analysis

The analysis of the root meristem organisation have been performed on wild type, three independent transformant lines of *pMP::MP* and three independent transformant lines of *pMP*::*MP11ir* at 5 days after germination. Roots were imaged by confocal microscopy using propidium iodate to visualise the cell walls. The images have been analyzed with the MorphoLibJ plugin[77] on Fiji ImageJ. By morphological segmentation the cells in the root tip have been identified as single labels. Subsequentially, the cells geodesic elongation was measured. The geodesic elongation is a shape descriptor whose value increases as an object became longer and narrower. The lowest value of geodesic elongation is 1 (associated to a disk).[84]

For the vascular Pattern analysis the wild type, the three independent transformant lines of *pMP::MP* and the three independent transformant lines of *pMP*::*MP11ir* were analyzed as described in.[85]

Root elongation assay

For root elongation on IAA added media, seeds for the wild type, three independent transformant lines of *pMP::MP* and three independent transformant lines of *pMP*::*MP11ir* were sown on half-strength MS media supplemented with either mock solution or IAA with a final concentration of 10nM, 100 nM, 300 nM or 1000 nM. After seed stratification, plates were transferred to the growing chamber. Pictures of the plates were taken from two days after germination until 5 days after germination. All the measurements were performed using Fiji ImageJ software.

RNA sequencing and data analyses

Roots from three independent lines pooled together for each complementation (*pMP::MP* and *pMP::MP11ir*) and from Wild type Col-0 were homogenized by Precellys Homogenizer (4000 rpm, 1 × 30 s) with TRIzol reagent and five glass beads in the tube. RNA was then isolated with the TRIzol method according to the product manual. DNA was digested by DNase I (NEB). RNA was double purified by LiCl precipitation, and the RNA pellet was washed twice with 70% EtOH before being resuspended in 30 μL RNase free water. The quality of RNA was checked by the RNA BR Tape and the concentration was determined by the Qubit BR RNA kit. RNA-seq libraries were prepared with 1 μg purified RNA using the TruSeq Stranded mRNA kit from Illumina, according to the kit manual.

Reads from the fastq files were trimmed and Illumina adapters removed using Trimmomatic (v0.36).[78] Resulting reads were mapped to the TAIR10 Arabidopsis genome using STAR v2.7.10a[79] with parameter values: alignIntronMax 6000; outFilterIntronMotifs RemoveNoncanonical; outSAMstrandField intronMotif; outSAMattrIHstart 0; outFilterMultimapNmax 2 and other parameters with default values.

featureCounts v2.0.1[80] was used to count the number of mapped reads per gene (in exon and introns) with default parameters. Raw read counts from 2 independent biological replicates per genotype (*pMP::MP*, *pMP::MP11ir* and wild type) were filtered with the R_HTS filter tool. Differential expression analysis was conducted using the Deseq2[81] R package using the wild type samples as normaliser. Differentially expressed genes with FDR $\leq$0.05 and |Log2FC|>0.6 were considered significant. DEGs plant ontology enrichment analysis was performed with the ShinyGo[57] webtool using the default configuration setting. Among the 106 MP direct targets,[24] the ones with FDR $\leq$0.05 and |Log2FC|>0 were considered differentially expressed. For MP direct targets expression distribution, percentage of expression enrichment in different tissue types[70] was calculated. *MP* and *MP* target genes expression was also evaluated with the bar.utoronto ePlant portal (https://bar.utoronto.ca/eplant/), using the available single-cell RNA seq dataset.[41]

Mathematical modeling

The methodology applied for the mathematical predictions is described in Methods S1.

Ubiquitination and sumoylation sites prediction

Putative ubiquitination sites prediction has been performed with the BDM-PUB web server (http://bdmpub.biocuckoo.org/index.php), using the default configuration settings. Putative SUMOylation sites prediction has been performed with the GPS-SUMO web server (http://sumosp.biocuckoo.org/), using the default configuration settings. In both cases, MP (AT1G19850) protein sequence in fasta format was downloaded from the UniProt database (https://www.uniprot.org/).

QUANTIFICATION AND STATISTICAL ANALYSIS

For Figures 1I, 3B, S2C, S3M, S3N, and S4E statistical significance has been presented with letters that indicate the results of one-way Anova with post-hoc Tukey HSD-test with $p < 0.05$. For Figure S5F, statistical significance has been presented with asterisks that represent the results of One-way Anova with post-hoc HSD test, showing the comparisons with the wild type. * = $p < 0,05$, ** = $p < 0,01$. For Figures 3G, 4K, 4L, 5G, and S7A–S7D, statistical significance has been presented with asterisks that indicate the results of t test student (two-tailed distribution, homoscedastic) confronting the mock with each treatment condition. * = $p < 0.05$, ** = $p < 0.01$, *** = $p < 0.001$.

For Figure 6E, statistical significance has been presented with asterisks that indicate the results of Pairwise Wilcoxon test. The black lines indicate the cell types that have been put in comparison. ** = $p < 0.01$, *** = $p < 0.001$. For the RNA-seq data, statistical significance has been evaluated using the Benjamini-Hochberg (FDR) test.

Statistical tests have been performed with Microsoft office Excel program, the online web tool Anova-atasta (https://astatsa.com/OneWay_Anova_with_TukeyHSD/) or with the R software. Details regarding the statistical tests used, sample size and number of independent biological replicates per each experiment can be found in the figure legends.